The Limiting Effects of Dust in Brown Dwarf Model Atmospheres

France Allard

Centre de Recherche Astronomique de Lyon (CRAL), Ecole Normale Supérieure de Lyon, Lyon, Cedex 07, 69364 France
E-Mail: fallard@ens-lyon.fr

Peter H. Hauschildt

Dept. of Physics and Astronomy & Centre for Simulational Physics, University of Georgia, Athens, GA 30602-2451
Email: yeti@hal.physast.uga.edu

David R. Alexander, Akemi Tamanai

Dept. of Physics, Wichita State University, Wichita, KS 67260-0032
E-Mail: dra@twsuvm.uc.twsu.edu

and Andreas Schweitzer

Dept. of Physics and Astronomy, University of Georgia, Athens, GA 30602-2451
Email: andy@physast.uga.edu

ABSTRACT

We present opacity sampling model atmospheres, synthetic spectra and colors for brown dwarfs and very low mass stars in two limiting case of dust grain formation: 1) inefficient gravitational settling i.e. the dust is distributed according to the chemical equilibrium predictions, 2) efficient gravitational settling i.e. the dust forms and depletes refractory elements from the gas, but their opacity does not affect the thermal structure. The models include the formation of over 600 gas phase species, and 1000 liquids and crystals, and the opacities of 30 different types of grains including corundum (Al_2O_3), the magnesium aluminum spinel $MgAl_2O_4$, iron, enstatite ($MgSiO_3$), forsterite (Mg_2SiO_4), amorphous carbon, SiC, and a number of calcium silicates. The models extend from the beginning of the grain formation regime well into the condensation regime of water ice ($T_{\rm eff} = 3000 - 100$ K) and encompasses the range of $\log g = 2.5 - 6.0$ at solar metallicity.

We find that silicate dust grains can form abundantly in the outer atmospheric layers of red and brown dwarfs with spectral type later than M8. The greenhouse effects of dust opacities provide a natural explanation for the peculiarly red spectroscopic distribution of the latest M dwarfs and young brown dwarfs. The grainless (Cond) models on the other hand, correspond closely to methane brown dwarfs such as Gliese 229B. We also

recover that the λ5891,5897Å Na I D and λ7687,7701Å K I resonance doublets plays a critical role in T dwarfs where their red wing define the pseudo-continuum from the I to the Z bandpass.

Subject headings: low mass stars,brown dwarfs,grains,fundamental parameters

1. Introduction

The discovery of the first unambiguous evolved brown dwarf Gliese 229B (Oppenheimer et al. 1995; Nakajima et al. 1995), the confirmation of the existence of young brown dwarfs in the Pleiades open cluster (Rebolo et al. 1996; Basri, Marcy, & Graham 1996; Zapatero Osorio et al. 1997), and the detection of dozens of others from photometric (Delfosse et al. 1997; Kirkpatrick et al. 1999b; Strauss et al. 1999; Tsvetanov et al. 2000) and proper motion surveys (Ruiz, Leggett, & Allard 1997b) has restricted the intriguing gap between stars and planets. In fact, brown dwarfs are bright enough to be easily detected in standard bandpasses ($ZJHK$) from ground-based facilities. This is now understood as the natural consequence of strong absorption bands of H_2O and H_2 that depress the infrared flux in favor of the near-infrared bandpasses, far from any black body distributions. This effect was already apparent from the results of our model atmospheres (Allard & Hauschildt 1995), which were later extended deeper into the temperature regime of evolved brown dwarfs by Allard et al. (1996). But as brown dwarf discoveries unfold, several questions arise. Why do brown dwarfs appear to form two distinct subgroups: 1) hotter red objects just below the stellar main sequence, and 2) much cooler and blue methane dwarfs? Is the apparent gap between these groups real? Are different physical processes involved in their atmospheres beyond the change of effective temperature?

From previous model atmospheres, it immediately appeared more difficult to explain the behavior of the hotter brown dwarfs, than that of the methane dwarfs in which water vapor and methane bands naturally matched the predictions of models ((Allard et al. 1996; Tsuji et al. 1996) and (Marley et al. 1996)) models within the accuracy of available molecular absorption profiles. Even the most detailed model atmospheres had failed to reproduce accurately the spectroscopic and photometric properties of red dwarfs later then about M6: all models were systematically too blue by as much as a magnitude in standard infrared colors ($V-K$, $I-K$, $J-K$). Allard et al. (1997) has reviewed this situation and the atmosphere modeling at the bottom of the main sequence. The reasons for these discrepancies was the onset of dust grain formation. As mass decreases along the main sequence, the latest-type red dwarfs bear outer atmospheric layers which reach temperatures well below 1800K, favoring the formation of dust grains. While it has been long suspected that grains could form under these conditions (Lunine et al. 1989), the inclusion of such computation to non-grey model atmosphere calculations had to wait until — using Gibbs free energies of formation (Burrows et al. 1993) and a simple sphere approximation for the Mie opacity of the grains — Tsuji et al. (1996) published their exploratory non-grey dusty brown dwarf models. They explored the

formation of three dust grain species: Al_2O_3, Fe, and $MgSiO_3$, and found corundum (Al_2O_3) to be a very abundant and powerful continuous absorber in red dwarfs with spectral type later than M8, while cooler methane brown dwarfs appeared comparatively grainless. But their models were based on band models for molecular opacities and could not reproduce the optical spectral distributions and several photometric properties of brown dwarfs.

Recently, Tsuji, Ohnaka, & Aoki (1999) and Ackerman & Marley (2000) have explored models with finite radial extention of silicate clouds to address the systematic difference between early L and late T type brown dwarfs. While it is pertinent to explore such processes, several parameters must inevitably be used to characterize them, and moreover, these are likely time-dependant processes (Bailer-Jones, & Mundt 2001, e.g. I-band variability has been recently detected in young brown dwarfs). So while we do believe that dust diffusion (referred to herafter as gravitational settling) contributes in reducing the radial extention of clouds in these atmospheres, we feel that, as in all unsolved physical problems, it is important to explore carefully the limiting cases. In this paper, we present therefore our model calculations for two opposite limiting cases of dust content in brown dwarfs atmospheres: 1) inefficient gravitational settling i.e. the dust is distributed according to chemical equilibrium predictions, which provides the maximum impact of dust upon the brown dwarf properties, and 2) efficient gravitational settling i.e. the dust forms and depletes refractory elements from the gas, but their opacity does not affect the thermal structure, hence a minimal effect upon brown dwarfs properties.

These models bring substantial improvements upon the previous similar work of Tsuji, Ohnaka, & Aoki (1996) in the number of grains included both in the chemical equilibrium and in the opacity database, as well as with regards to the molecular opacities. In Section 2 we describe how hundreds of grain species are now included self-consistently to the chemical equilibrium calculation to allow us to identify the hot condensates that are most abundant in the atmospheres of late-type M dwarfs and brown dwarfs. In Section 3 we describe our treatment of the grain opacities. And Section 4 we describe the detailed opacity sampling model atmospheres to which these grain formation and opacities are incorporated. Section 6 is reserved for the discussion of the atmospheric structures, while the effects of grains on the spectroscopic and photometric properties of brown dwarfs are discussed in Section 7 and 8.

2. Condensation and the Chemical Equilibrium

The chemical equilibrium (hereafter CE) of the atmosphere code Phoenix already solves simultaneously for 40 elements with usually 2 to 6 ionization stages per element, and 600 molecular species relevant for oxygen-rich ideal gas compositions. This CE has been gradually updated since Allard & Hauschildt (1995) with additional molecular species using the polynomial partition functions by Irwin (1988) and (Sharp & Huebner 1990, , hereafter SH90). The molecular ions TiO^+ and ZrO^+, which have been found to be important in the balance of TiO and ZrO when departures from local thermodynamic equilibrium are present (Hauschildt et al. 1997), have been added using

the partition functions by Gurvich & Glushko (1982). The ions H_3^+ (and H_2^+), which are important electron donors in low metallicity subdwarf stars and white dwarfs (Saumon et al. 1994, see), has been added to our CE and opacity database by using the partition function by Neale & Tennyson (1995) and a list of 3 million transitions by Neale, Miller, & Tennyson (1996).

To include dust grains, we have expanded the system of CE to include the complete series of over 1000 liquids and crystals also studied by SH90. For each grain or liquid species, we followed the prescriptions of Grossman (1972) and used Gibbs free energy of formation $\Delta G(T)$, drawn from the JANAF 1986 database Chase et al. (1985), to compute the so-called equilibrium pressures $P_{eq} = \exp^{-\Delta G(T)/RT}$ of the grains, where R is the gas constant and T the local gas temperature. P_{eq} was then compared to the pressure, P_c, obtained from the Guldberg law of mass-action (i.e. the product of the pressures of the constituting elements). The abundance of a condensed species was then determined by the condition that this species be in equilibrium with the gas phase, $P_c \geq P_{eq}$. For corundum,

$$P(Al_2O_3) = \frac{P(Al)^2 P(O)^3}{P_{eq}} P(Al_2O_3)^{max};$$

$$for\ P_{eq} \leq P(Al)^2 P(O)^3$$

where max refers to the maximum concentration of grain cores (one core of corundum = one Al_2O_3 unit) given the conservation of the cores of each elements. The complete CE was then solved by Newton-Raphson iteration of the equation system (Allard 1990; Allard & Hauschildt 1995, see also) until the error relative to the gas pressure of all partial pressures was below -6 dex. The computations were then performed and tabulated in a $[P,T]-$plane encompassing largely the conditions prevailing in low mass stars and brown dwarfs ($P = -4$ to 12 and $T = 15000$ to 10K), using a solar mix (Grevesse & Noels 1993) except for lithium (meteoretic abundance, same source). The CE tables were then interpolated in the construction of the model atmospheres.

The CE therefore accounts, self-consistently, for the depletion of refractory elements as a function of the gas temperature and pressure conditions in the model atmospheres. However, it should be clear that thermodynamic equilibrium studies only tell us what can be formed, not what is formed. And the results are only as certain as the JANAF equilibrium constants on which they are based. In favor of CE, note however that Lodders & Fegley (1998), who used thermodynamics, were able to explain the abundance patterns of various trace elements dissolved in carbide stardust. We therefore feel confident that our CE calculations allow us at least to reproduce, in average, adequately the limiting thermal and spectroscopic properties of brown dwarfs. However we do not claim that this CE calculation predicts exactly the distribution of dust species in brown dwarfs atmospheres. Gravitational settling effects would certainly change this distribution. We note in passing that our main results (Allard & Hauschildt 1995, ,and present) concur with both those of Lodders (1999) and Tsuji (1973). This consistency between independent CE works is reassuring.

In this work, contrary to recent calculations by Burrows & Sharp (1999), we have not attempted to handle the effects of gravitational settling (i.e. diffusion of the grains to lower atmospheric layers). We do not account for elemental abundance depletion resulting from dust grain settling. This process is likely important in the uppermost layers of brown dwarf atmospheres, and would tend to deplete these layers of their refractory elements and dust grains. However, the error introduced by this omission on the models presented in this paper is small since these represent limiting cases with non-existent and complete settling, where the dust opacity has been ignored altogether to recreate the latter case. The available abundance of refractory elements involved in dust formation can however be slightly overestimated. The complete treatment of gravitational settling goes beyond a simple parametrization of the problem, and involves solving the diffusion of the dust as a function of the characteristic timescale of several important processes such as the sedimentation, coagulation, condensation and convective mixing of the dust. This work is, however, under development and we will present our findings in a separate publication.

Since the predictions of CE calculations have been described in detail by Tsuji (1973) and Lodders (1999), we do not deem necessary to develop this here again. Yet the completeness of the grain species sample included here (within the limits of the CE approximation and JANAF data) provides an opportunity to explore some of the effects of condensation upon the composition of late-type dwarf stars and brown dwarfs atmospheres. In the atmospheres of brown dwarfs, most of the hydrogen is locked in H_2, most of the oxygen is in CO, H_2O and SiO, and most of the carbon is in CO and CH_4. The species responsible for the strong optical to near-infrared (0.4 to 1.1 μm) opacities in M dwarf stars and young brown dwarfs are relatively trace species much less abundant then CO or H_2O, which have large opacity cross-sections per molecule. The relative abundance of those species are summarized in Figure 1 and 2 which illustrate the nature and progression of the condensation layers into deeper layers of the photosphere[1] as $T_{\rm eff}$ decreases. At a $T_{\rm eff}$ = 2600 K which is typical of the young Pleiades brown dwarfs Teide1 and Calar3 (Zapatero Osorio et al. 1997, see), the clouds barely touch the top layers of the photosphere which is located between $\tau_{1.2\mu m} = 10^{-4}$ to 1 depending on the spectral range considered. As can be seen from the inner to outer atmospheric regions (right to left on the plots), the first species to condense at T$\approx$ 2000K is ZrO_2, followed by corundum (Al_2O_3) at T$\approx$ 1800K. We clearly identify the perovskite $CaTiO_3$ as the source of depletion of TiO, the principle optical absorber in these atmospheres. However, the depletion occurs in this model only above the photosphere and should leave the spectra relatively unaffected. Other stable species to appear at T$<$ 1600K are $MgAl_2O_4$, $CaSiO_3$, Ca_2SiO_4, $Ca_2Al_2SiO_7$, $Ca_2MgSi_2O_7$, and $CaMgSi_2O_6$, as well as Ti_4O_7 and Ti_2O_3. These grains all compete with the formation of $CaTiO_3$ and corundum, and form an intricate layer of clouds just above the photosphere. Note that, contrary to the reports by Tsuji, Ohnaka, & Aoki (1996), corundum is *not* the most abundant grain species and even disappears in central regions of the clouds.

[1]In this paper we refer to the photosphere as the part of the atmosphere which encompasses the entire optical depth range where the spectrum forms, from the visible to the infrared ($\approx \tau = 10^{-4}$ to 1.0).

The situation complicates rapidly as T_{eff} decreases. Figure 2 shows how the clouds have already invaded most of the photosphere in brown dwarfs of about 1800K typical of field brown dwarfs such as GD165B Becklin & Zuckerman (1988), Kelu1 Ruiz, Leggett, & Allard (1997b) or the DENIS objects Delfosse et al. (1997). Dozens of new grain species including iron, enstatite ($MgSiO_3$) and forsterite (Mg_2SiO_4) are now present. The photospheric gas phase abundances of TiO, FeH, and CaH (not shown) are now strongly depleted. This is reflected by the gradual disappearance of these features in the latest-type M dwarfs and brown dwarfs, a behavior which is already apparent from the observed spectra of brown dwarf candidates BRI0021, GD165B and Kelu1. The VO abundances seem, on the other hand, much less depleted by the condensation of VO and V_2O_4 occurring only in the upper photosphere. And other compounds of less-reactive elements such as Li, K, Rb, Cs, and CrH are left relatively unaffected, favoring the detection of their features in these objects.

Between T_{eff} = 1800 and 1000 K, methane (CH_4) gradually forms at the expense of CO. The likelihood of detecting methane lines in the spectra of cool brown dwarfs depends therefore on the height in the atmosphere where this transition regime occurs, and depends upon T_{eff}, gravity, and dust opacity conditions such as gravitational settling, rotation, winds, etc.

Although the clouds appear to persist in Figures 1 and 2 out to the outer edge of the photosphere in our coolest models, this only reflects the omission, mentioned above, of the gravitational settling of the grains. Clouds form more likely in thin decks above the deepest condensation layer in brown dwarfs (Tsuji, Ohnaka, & Aoki 1999; Ackerman & Marley 2000, see e.g.).

The principle impact of condensation on the photospheres and spectra of cool dwarf is a gradual depletion of their refractory elements, especially zirconium, titanium, silicon, calcium, magnesium, aluminum, iron and nickel. Clearly, it is crucial for the balance of the opacities in the models to account for the leading grain species in the chemical equilibrium. Partially accounting for condensation leads to errors of several orders of magnitudes in the model opacities and predicted fluxes. See Allard (1998) for a comparison between existing dusty models. To fully understand the spectroscopic and photometric properties of brown dwarfs, one must also consider the optical and radiative properties of dust grains.

3. Dust Clouds Construction and Opacities

In this paper, we account for the dust opacity only in the limiting case of the AMES-Dusty models where gravitational settling is neglected and which are relevant for the analysis of hot red dwarfs. In these models, cloud layers build up automatically following the condensation equilibrium which determines the atmospheric layers occupied by the grains. The study of the jovian planets suggests that cloud layers are not generally distributed homogeneously over the atmospheric surface. But if the nucleation process of dust grains is favored by a combination of high gas densities and low gas temperatures, hotter red dwarfs could be expected to retain more easily smaller grains in their photosphere, and have them more uniformly distributed over the stellar surface. In this work,

we account for the average effect of the presence of clouds on the model structures and emitted spectra. We therefore assume a plane-parallel symmetry, i.e. an homogeneous distribution of clouds across the surface of the brown dwarfs. The spectral distribution of a brown dwarf with a more complex ring pattern of clouds familiar to jovian planets could, in the end, be reconstructed from a mosaic of the present models until a full three dimensional calculation becomes possible.

Early attempts to compute the opacities of grains were made by Cameron & Pine (1973) and Alexander (1975). More detailed calculations, including the effects of chemical equilibrium calculations and grain size distributions were reported by Alexander, Johnson, & Rypma (1983) and Pollack, McKay, & Christofferson (1985). Alexander & Ferguson (1994) have described the computation of the opacity of grains with the inclusion of equilibrium condensation abundances, the effects of the distribution of grain sizes, and the effect of grain shape through the Continuous Distribution of Ellipsoid (CDE) model of Bohren & Huffman (1983). These calculations included the absorption and scattering due to magnesium silicates, iron, carbon, and silicon carbide grains for a wide range of chemical compositions down to 700 K. We have explored the CDE method employed by Alexander & Ferguson, but have retained a purely spherical shape of the grains in the present study for simplicity. Another difference with Alexander & Ferguson is that, instead of approximating the number density of grains indirectly, these quantities are now provided by our chemical equilibrium as described in Section 2. 26 new condensates have been added to the original list of Fe, C, SiC and magnesium silicates, for a total of 30 among which are $MgSiO_3$, Mg_2SiO_4, Al_2O_3 and $MgAl_2O_7$, using polarizability constants from laboratory studies by Tropf & Thomas (1990), Koike et al. (1995), Begemann et al. (1997), and Dorschner et al. (1994). Figure 1 and 2 suggest that the calcium silicates can also play an important role in the opacity of brown dwarf atmospheres. In fact, complex calcium silicates (here $Ca_2Al_2SiO_7$, $Ca_2MgSi_2O_7$, and $CaMgSi_2O_6$) are amoung the most abundant species in the layers where these grains are present. Since, for the latter two species, no data were available to construct their opacity profiles, we have simulated their opacity using the profile of $Ca_2Al_2SiO_7$. We includes in general, more accurate number densities, and better and more complete cross-sections of dust grains than included in Alexander & Ferguson (1994). Updated Rosseland and Planck opacities computed with these updated opacities will be published in more details separately (Alexander et al. 2000).

The opacity profiles of these grains are shown in Figure 3. Most spectral distributions seen in this plot are pure absorption profiles. Scattering contributes only at UV to optical wavelengths for the grain sizes adopted. Corundum, enstatite, forsterite, hematite, magnetite, and $Ca_2Al_2SiO_7$ have absorption cross-sections exceeding those of water vapor. In a brown dwarf atmosphere, however, water is at least two orders of magnitudes more abundant then most of these grain species, so that water vapor remains the leading opacity source between 1 and 8 μ, and beyond 20 μm. In other words, grains do not contribute significantly to the opacities in the near-infrared where water bands still dominate the brown dwarf spectra from J to K (1.0 to 3 μm). We have demonstrated in Section 2 that grain species have concentrations similar to those of TiO, VO and most other optical absorbers. The impact of the grain opacities is, therefore, to enhance and gradually replace

the optical opacities as these gas phase species disappear via condensation.

The extinction caused by grains in a stellar atmosphere also depends on the rate of grain formation and the resulting size distribution. For all grains included we have assumed, as in Alexander & Ferguson, an interstellar size distribution of the grains with diameters ranging from 0.00625 to 0.24 μm. For comparison, Tsuji, Ohnaka, & Aoki (1996) and Tsuji et al. (1996) assumed grains with a fixed diameter of 0.1 μm in their model atmosphere calculations. Although those choices are purely arbitrary, the consequences are minimal since the grain diameter cancels out in the opacity calculations as long as: (1) abundance conservation is assumed i.e. larger grains must lock more particles, reducing the number of grains per gram of stellar plasma, and, (2) that the cross-sections behave in the Rayleigh limit, i.e. the wavelength is larger than the size of the grains. Our tests, shown in Figure 4, confirm that this is the case for 1 to 10 μm-size grains, but they also indicate that the scattering increases rapidly for sizes larger than 10 μm, i.e. when the Rayleigh limit beaks down over the wavelengths carrying flux in these objects. But even is the opacities are sensitive to the grain sizes beyond the Rayleigh regime, the enormous scattering effects seen for 100 μm grains in Figure 4 seems to exclude the presence of such grains in brown dwarfs. We therefore believe that such large grains tend rapidly to become larger by coagulation to be eliminated by sedimentation in these high-gravity atmospheres. An accurate answer to this question can only come from time-dependent grain growth calculations incorporating the effects of sedimentation, diffusion, coagulation and coalescence for the conditions prevailing in brown dwarfs atmospheres. See Alexander et al. (2000) for a detailed description of the dust opacities used in the present models.

4. Molecular Opacities

Molecules dominate the spectral distribution of brown dwarfs. Young brown dwarfs hotter then 2000K emit flux principally in the near-infrared ZJHK bandpasses from 0.9 to 2.5 μm with bands of water steam in the infrared and TiO and VO bands in the optical shaping each side of this spectral distribution. Below 2000K, TiO, VO and CaH bands vanish as a result of the condensation of these refractory elements and the collision-induced opacities of H_2 and the growth of CH_4 bands become increasingly important in the H, K and L bandpasses at 1.6, 2.0, and 3.5 μm. It is this situation that causes the radiation to remain forced to emerge principally from the near-infrared bandpasses rather than emerging redwards as black bodies would do. Several other molecules are also present in brown dwarf spectra; overtones of CO at 2.3 and 4.7 μm are strong $T_{\rm eff}$ indicators and play an important cooling role upon the upper atmospheric structure, vibrational bands of SiO and hydrides such as OH, SiH and MgH determine the ultraviolet and visual radiation, the Wing-Ford system of FeH at 0.98 μm is one of the most prominent features in the spectra of late-type stars and young and/or massive brown dwarfs.

Our molecular opacity data base includes (i) a list of 43 million atomic transitions by Kurucz (1994), (ii) Collision-Induced Absorption (CIA) opacities for H_2, He, H, N_2, Ar, CH_4, and CO_2 by

(Borysow, Jorgensen, & Cheng 1997a,b; Borysow & Frommhold 1986a, 1987a, 1986b; Borysow & Tang 1993; Samuelson, Nath, & Borysow 1997; Borysow & Frommhold 1986c, 1987b; Gruszka & Borysow 1997, and references therein), (iii) ab initio line lists for H_2O and TiO by Partridge & Schwenke (1997); Schwenke (1998), (iv) CO from the line list by Goorvitch & Chackerian (1994a,b), Goorvitch (1994), (v) most other molecular systems such as MgH and OH are included from the list by Kurucz (1993), (v) VO and CrH lines have been calculated by R. D. Freedman for this work, while (vi) FeH lines from Phillips & Davis (1993) have been also included. For the remaining molecular band systems for which no line lists were available to us (CaH) we apply the Just Overlapping Line Approximation (JOLA) as described and utilized by (Tsuji 1995; Tsuji, Ohnaka, & Aoki 1996; Tsuji et al. 1996, and references therein).

We have also included a combination of the `HITRAN92` and GEISA databases (Rothman et al. 1992; Husson et al. 1992) summing up to about 700,000 lines of 31 molecules with a total of 74 isotopes. The molecules with the largest number of lines which are included in our models are O_3 (168,881 lines), CO_2 (60,790), and CH_4 (47,415). This database only includes the strongest lines of these molecules. However, the gf-values and position of the lines have comparatively high accuracy and allow us to diagnose their importance in brown dwarf atmospheres. A comparison of models computed with these opacities to the NextGen models Hauschildt, Allard, & Baron (1999); Allard et al. (1997) can be found in Allard, Hauschildt, & Schwenke (2000a).

5. The Model Atmosphere

We use the model atmosphere code `PHOENIX` (version 10.8). The original versions of `PHOENIX` were developed for the modeling of novae and supernovae ejecta described by (Hauschildt & Baron 1999, and references therein), and is dotted of a detailed radiative transfer (Hauschildt 1992) that allows for spherical symmetry. Its more recent application to cool dwarfs is described in detail by Allard & Hauschildt (1995); Hauschildt, Allard, & Baron (1999), and has served to generate grids of stellar model atmospheres which successfully described low mass stars in globular clusters (Baraffe et al. 1995, 1997) and the galactic disk main sequence (Baraffe et al. 1998). These former model grids are known to the stellar community as the 1995 Extended and the 1996-1999 NextGen models, and allowed a preliminary incursion into the regime of evolved brown dwarfs down to $T_{\rm eff} = 1600\,K$ (Extended models) and to 900K (Allard et al. 1996). These models successfully predicted the general spectroscopic properties of evolved brown dwarfs *prior* to the discovery of Gliese 229B, which then helped confirm its very cool brown dwarf nature (Allard 1995). Yet the lack, in these essentially stellar models, of dust condensation in the chemical equilibrium made them inadequate to model in detail such cool objects.

The addition to `PHOENIX` of the treatment of condensation in the chemical equilibrium, and of dust clouds, as described in Sections 2 and 3, was completed in 1996 (Allard 1998; Allard et al. 1998; Allard, Alexander, & Hauschildt 1998), and served to compute M dwarfs and brown dwarfs model atmospheres, synthetic spectra and broadband colors for specific analysis (Leggett et al.

1996; Ruiz, Leggett, & Allard 1997b; Tinney et al. 1998; Leggett, Allard, & Hauschildt 1998; Martín et al. 1998; Kirkpatrick et al. 1999a; Leinert et al. 1999; Leggett et al. 2000; Basri et al. 2000) and interior models (Chabrier et al. 2000). In this paper we present the final version of these models in two limiting cases: (1) "AMES-Dusty" which include both the dust formation in the chemical equilibrium and opacities, and; (2) "AMES-Cond" which include the effects of condensation in the chemical equilibrium but ignores the effects of dust opacities altogether. This latter case is computed to explore the case where dust grains have formed, but have disappeared completely (eg by sedimentation i.e. settling below the photosphere). These two model sets also distinguish themselves from the standard NextGen models by the use of the NASA AMES H_2O and TiO line lists while the NextGen models were computed using the Jørgensen (1994); Schryber, Miller, & Tennyson (1995) line list. This choice is motivated by the incompleteness of the 1994 lists to high gas temperatures ($T_{gas} > 2000$K) as discussed in Allard, Hauschildt, & Schwenke (2000a).

For the purpose of this analysis, we use the radiative transfer in plane-parallel mode. The convective mixing is treated according to the Mixing Length Technique (MLT). We consider pressure-dependent line-by-line opacity sampling treatment for both atomic and molecular lines in all models. We do *not* pre-tabulate or re-manipulate the opacities in any way: `PHOENIX` includes typically $\approx 15 \times 10^6$ molecular and atomic transitions which are re-selected at each model iteration and each atmospheric depth point from our data base described above. The lines are selected from three representative layers of the atmosphere at each model iteration to ensure consistency of the calculation. Van der Waals pressure broadening of the atomic and molecular lines is applied as described by Schweitzer et al. (1996). We neglect the effects of convective motion on line formation since the velocities of the convection cells are too small to be detected in low-resolution spectra and will have a negligible influence on the transfer of line radiation.

A trial atmospheric profile is applied, the equations of hydrostatic and radiative transfer are solved, and the solution is tested until convergence is reached. The model is considered converged when the energy is conserved within a tenth of a percent from layer to layer. At each of the model iterations, a spectrum with typically over 30,000 points is generated which samples the bolometric flux from 0.001 to 500 μm with a step of 2Å in the region where most of the flux is emitted (i.e. 0.1 to 10 μm). The final spectrum must generally be *degraded* to the instrumental resolution before being compared to low-resolution observations of stars and brown dwarfs. The model atmospheres are characterized by the following parameters: (i) the surface gravity, $\log(g)$, (ii) the effective temperature, $T_{\rm eff}$, (iii) the mixing length to scale height ratio, α, here taken to be unity, (iv) the micro-turbulent velocity ξ, here set to $2\,{\rm km\,s^{-1}}$, and (v) the element abundances taken from Grevesse & Noels (1993).

For this paper we have calculated a uniform grid of AMES-Cond models ranging from $T_{\rm eff}$ = 3000 to 100K in 100K steps, and with gravities ranging from $\log g = 2.5$ to 6.0 in steps of 0.5 dex at solar metallicity. The AMES-Dusty grid was calculated from $T_{\rm eff}$ = 3000 to 1400K in steps of 100K, with gravity ranging from $\log g = 3.5$ to 6.0 in steps of 0.5 dex. All models were fully converged.

Although PHOENIX can treat the effects of external radiation fields on the model atmosphere and the synthetic spectrum (Baron et al. 1993), we assume here a negligible external radiation field for simplicity. It is clear, however, that UV radiation impinging on the brown dwarf, from a hotter companion, will change the structure of the atmosphere and the corresponding spectra. We are investigating these effects in a separate publication (Barman, Hauschildt, & Allard 2000).

6. Atmospheric Structures and Convection

The photospheric thermal structures of the AMES-Cond models with $T_{\rm eff}$ ranging from 3000 to 100K are displayed in Figure 5. The convection zones are labeled with cross-symbols. As $T_{\rm eff}$ decreases, the photosphere becomes progressively more isothermal. While the convection zone retreats to deeper layers down to $T_{\rm eff} = 1000$K, an outer convection zone begins to form in the clouds until this zone detaches itself from the inner convection regime in models cooler than 500K. Meanwhile, the inner convection continue to retreat inwards. This appears to confirm qualitatively earlier work by Guillot et al. (1994) and (Burrows et al. 1997). Yet even in our coolest models, the inner convection zone always reaches at least up to an optical depth of $\tau_{1.2\mu m} = 10$. For $T_{\rm eff} = 1000$K for example, the convection zone seems to be quite deeper in Burrows et al (1997) models (roughly $P_{gas} > 100$ bar as seen from their Figure 5) than in our models. Note that we treat the convection according to the Mixing Length Theory from the onset of the Schwarzchild criterion while Burrows et al (1997) assumed a pure adiabatic mixing throughout the convective unstable zones. But this appears to be a valid approximation since our calculations indicate that the true temperature gradient as predicted by the MLT remains within 0.05% of the adiabatic gradient value at each layer. So the difference appears to lie in the opacities included in the construction of the respective models: their models would be more transparent to radiation than ours.

The optical resonance lines of K I and Na I D also contribute significantly to the optical opacity and the heating of the atmospheric layers. We have explored their impact on the thermal structure of a $T_{\rm eff} = 1000$K, $\log g = 5.0$, solar composition model. It appears that their opacity contribution accounts for 100 and 300K of heating in the photospheric ($\log P = 5.5$) and internal ($\log P = 8.5$) layers respectively. The models become unstable to convection further out when atomic lines are included ($\log P = 7.76$ versus 8.1). And uncertainties in the applicability of Lorentz profiles (estimated from models computed with restricted coverage of the line wing opacity contributions) produce a corresponding uncertainty of less than 40K in the photosphere and 150K in the internal layers. These uncertainties are therefore of little importance for the synthetic spectra and evolution models, compared to those tied to the treatment of the dust (Cond vs Dusty), and incomplete molecular opacities (e.g. H_2O opacity profile. See Allard, Hauschildt & Schwenke, 2000). However, neglecting the K I and Na I D doublet opacities altogether in the construction of the thermal structures has a greater impact and fully explains the difference between our models and those of Burrows et al (1997). Indeed, while our model at $T_{\rm eff} = 500$K and $\log g = 5.0$ do not present detached convection zones, we reproduce exactly the several detached convection zone

found by these authors when neglecting atomic line opacity in the model construction. We must conclude from this that these opacities were neglected in their work. The reality of the occurrence of detached convection zone is therefore likely closer to our predictions.

The thermal structures of the fully dusty AMES-Dusty models over the $T_{\rm eff}$-range where dust begins to form (2500 to 1500K) are displayed in Figure 6 at constant gravity. The convection zone, marked by dotted lines, extends out to T_{gas} = 2500K is all these models. This corresponds to optically thin layers in models hotter than 1600K. Even down to 500K, these dusty atmospheres never become fully radiative. But the interesting part is what happens to photospheric regions as grain opacities begin to heat up the outer layers. Within the photosphere (marked by with full circles and triangles), the temperature normally decrease smoothly with decreasing $T_{\rm eff}$, and the thermal structures parallel for grainless models. Here, the greenhouse effect of the dust tends to raise the temperature of the outer layers increasingly with decreasing $T_{\rm eff}$. This has for effect that the outer structures level off between $T_{\rm eff}$ = 2600 and 1800K to a T_{gas}-value in a narrow range between 1280 and 1350K. The slope of the thermal structure in the line forming region becomes therefore increasingly flatter in that $T_{\rm eff}$-range. Below 1800K, the greenhouse effect saturates and the outer thermal structure resumes its decrease in temperature with decreasing $T_{\rm eff}$. It is interesting to note that 1800K is also the break-up temperature where full-dusty atmospheres become unrealistic in modeling brown dwarfs. This can be seen from Figure 6 of Chabrier et al. (2000) and from Section 8 below. We believe that grains sedimentation has certainly started at these temperatures as also concluded by Lunine et al. (1989), Burrows & Sharp (1999) and Ackerman & Marley (2000).

7. Synthetic Spectra

In Figure 8 we display the spectral sequence of brown dwarfs to extrasolar giant planets (hereafter EGP) model atmospheres from $T_{\rm eff}$ = 3000 to 200K in the total gravitational settling (AMES-Cond) approximation. All dust opacity is neglected, but also all optical molecular opacity sources disappear due to the condensation of species involving Ti, V, Ca and Fe (TiO, VO, CaH, FeH, etc.), making these models transparent to the emergent radiation bluewards of 1.0 μm. Because of the absence of dust opacity, the photospheric layers are very cool compared to non-depleted atmospheres. The formation of optical atomic resonance lines and infrared molecular bands is then favored. We observe that water vapor bands (0.93, 0.95, 1.2, 1.4, 1.8, 2.5, and 5-10 μm in the window shown by this plot) increase rapidly in strength. Another striking consequence of the cool photospheric temperatures is the formation of CH_4 bands (3.5 and 6-10 μm, with weaker bands at 1.6 and 2.2 μm appearing in cooler models) already at 2000K. Methane gradually replaces water vapor bands while H_2O condenses out to ice below 300K.

One major feature of the AMES-Cond model spectra is the extraordinary growth of atomic resonance absorption lines at short wavelengths. Burrows, Marley, & Sharp (2000) have explored grainless models of methane dwarfs and found that van der Waals broadening of K I and Na I resonance optical lines can extend to several thousands of Angstroms on each side of the line cores.

Our models behave similarly. Figure 9 shows how the van der Waals wings of the Na I D and K I resonance lines at λ5891,5897Å and λ7687,7701Å completely depress the optical flux of cool brown dwarfs. In this case ($T_{\rm eff}$ = 1000K, $\log g$ = 5.0), the wings extend largely over 7000Å on each side of the line center. This is as large as hydrogen Balmer line wings in cool white dwarfs! However, to our knowledge, it is the first case of such behavior in metal lines encountered in stellar astronomy. While the van der Waals collisional C6 damping constant may be sufficiently accurate for the treatment of alkali element lines in the hydrogenic approximation in low mass stars and red dwarfs where these lines rarely exceed a width of 50Å, this treatment becomes questionable under these unprecedent conditions as also concluded by Burrows, Marley, & Sharp (2000). Here, we observe for example that the red wings of these transitions prevents even a fraction of the flux from escaping in the J-band window around 1.25 μm, while observed spectral distributions of methane dwarfs tend to carry more flux in this window. The reason for such large line broadening is not the decreasing $T_{\rm eff}$ of the photospheric gas pressure. It is rather, as also observed by Allard (1990); Allard & Hauschildt (1995); Tinney et al. (1998) for metal-depleted atmospheres, the result of the increasing transparency of the atmosphere which allows us to see deeper into the structure to inner high pressure depths. The line wing flux integrates therefore over an increasingly large column density of the atmosphere as optical molecular opacities vanish via condensation.

Figures 10 and 11 display the change of the optical to red spectra as a function of temperature, where the gradual disappearance of TiO, VO, FeH, and CaH bands (by condensation of related species) and gradual strengthening of optical Na I D and K I lines becomes obvious. The TiO band systems (λ0.545, 0.616, 0.639, 0.665, 0.757, 0.774, 0.886 μm) become undetectable below 2000K, while the MgH (λ0.513 μm), CaH (λ0.694 and 0.706 μm), VO (λ0.829, 0.848 and 0.961 μm), FeH (λ0.990 μm) bands persist down to 1500K. The CrH bands at λ0.861 μm, already visible at 2500K in these AMES-Cond models, grow in strength as $T_{\rm eff}$ decreases until it disappears by condensation of Cr_2O_3 below 900K. However, we must point out that red dwarfs are heavily reddened by dust opacities at least down to $T_{\rm eff}$ = 2000K, so that the Cond models overpredict the strength of CrH bands over that temperature range. Still, clearly the CrH bands become one of the strongest molecular system to be observed in the red spectra of cooler brown dwarfs.

From 2000K, we also see the H_2O band system at λ0.927 μm becoming increasingly stronger. The Na I D resonance doublet remains visible down to 400K, and K I already begins to get locked into dust below about 900K, a temperature typical of currently known methane dwarfs such as Gl229B. Other features growing in strength as $T_{\rm eff}$ decreases are the lines of alkali elements such as Li I at λ6708Å, Rb I at λ7802 and 7949Å, Cs I at λ8523 and 8946Å, and Na I at λ8185Å. We also note the presence of diagnostic lines further in the near-infrared such as the K I doublet at λ11693,11776 and λ12436,12525Å,and a Na I line at λ11409Å.

The λ6708Å Li line, normally used to determine the substellar nature of brown dwarfs (Rebolo, Martin, & Magazzù 1992), remains detectable down to 700K. The Na I. Rb I and Cs I lines keep increasing in strength, but this is likely an artifact of the inevitable incompleteness of thermochemical databases in the construction of the chemical composition at these temperatures.

Thanks to R. Freedman (NASA-Ames), we were able to replace the band model approximation by a detailed line list for VO besides also being able to include CrH lines for which we had no previous counterparts. The result is that the present models show weaker VO bands, relative to TiO, strength than in previous models. A detailed comparison to high resolution observations of M and brown dwarfs is being published separately (Schweitzer et al. 2000). However, note that the VO line list does not include C-X system at 0.75 μm. Our current models, therefore, overestimate the flux in the 0.75 μm region.

In Figure 12, we explore the behavior of the 4.55 μm CH_3D band system between $T_{\rm eff}$ = 2000 and 400K. At those wavelengths, H_2O provides the pseudo-continuum absorption. In the limit of the Cond models, CH_3D is practically undetectable until it begins to grow from 1000K to lower effective temperatures. The ammonia band at around 11 μm behaves similarly as can be seen from Figure 13. This is a result of the growing transparency of the atmosphere while water begins to condense in the uppermost layers of these Cond models. Note that although CO bands at 4.67 μm are not visible in Cond models with $T_{\rm eff} \geq$ 1800K, these bands do appear in corresponding brown dwarfs and stars. This is because the Cond limit does not apply for those dusty dwarfs.

In Figure 14, we present the full dusty (AMES-Dusty) limiting case from 2500 to 1500K. Here the strong heating effects of dust opacities prevent the formation of methane bands, and H_2O is dissociated while producing a hotter water vapor opacity profile, much weaker and more transparent to radiation. From 1700K, the grain opacity profiles rapidly dominate the UV to red spectral region, smoothing out the emergent flux into a continuum. Only the cores of the strongest atomic resonance lines (Na I D and K I) can be seen. The result is a spectral distribution guetting closer to the equivalent blackbody distribution of same effective temperature (see also Figure 20). Note however, that Dusty models can never be approximated by blackbodies because of the important optical-to-red dust veiling, and the strong near-IR water vapor bands. We have explored the effects of grain sizes on these models and found that for grains with sizes in the submicron to micron range, the increased cross-sections are compensated by the corresponding reduction in the number density of these grains given the conservation of the elemental abundance. For grains with sizes beyond 10 μm, an increased global opacity is found which produces even redder models. But grains are likely to be distributed in a spectrum of sizes where the balance between coagulation, sedimentation and condensation decides the upper limit of the masses reached. Preliminary calculations (T. Guillot, private communication) which will be published separately show that, when accounting for all the relevant processes, the grain sizes remain in the submicron range. We are therefore confident that the current models with grain sizes in the submicron range do constitute an adequate full dusty limit for these dwarfs.

7.1. Gravity

In Figure 15 and 16, we explore the effects of surface gravity on AMES-Cond models with $T_{\rm eff}$ = 2500 and 500K. At 2500K, gravity sensitivity is essentially noticeable in hydride bands

(CaH at 0.624 and 0.639 and FeH at 0.98 μm) while the oxide bands (TiO and VO) form too high in the atmosphere ($\tau_{\rm std} = 10^{-4}$) to be affected except in interband pseudo-continuum regions. Effects of gravity are however more extensive in the strength of atomic lines (essentially K I and Ti I) at the peak of the spectral distribution (1.05 to 1.3 μm), and in the red wing of the water vapor bands as well as in the CO bands at 2.3 to 2.4 μm. In the 500K case, H_2O bands are only moderately affected by the gravity change, while the optical continuum opacity, provided by the van der Waals wings of the Na I D and K I resonance doublets, is reduced by nearly a factor of 10 in the 500K in the low gravity case in response to the drop in pressure. The most interesting feature is the enhanced sensitivity of the K-band flux at 2.2 μm to gravity. As already pointed out by Allard et al. (1996), this feature can be used to disentangle temperature, age and mass of a brown dwarf or planet independently. This trend is observed in the entire regime from 1500K to 300K, and provides a useful tool in the analysis of free floating methane dwarfs such as discovered recently by Strauss et al. (1999) and Tsvetanov et al. (2000). The CH_4 and CO bands are also sensitive to gravity in this regime.

One more gravity indicator should be the slope and height of the Z-band flux between the core of the K I resonance doublet at λ7687,7701Å to 1.1 μm compared to the height of the J-band flux peak. However, for the reasons mentioned above, it is difficult to quantify this effect on the basis of the present models.

Surface gravity effects have also been explored for the fully dusty case (AMES-Dusty models) at $T_{\rm eff}$ = 2000 and 1500K (see Figures 17 and 18). In the 2000K case, the pseudo-continuum formed by saturated bands of TiO bluewards of 0.75 μm is fainter and flatter at reduce gravity. This is a result of the cooler temperatures prevailing in the outskirts of the photosphere at reduced gravity. This explains and supports the conclusions of Martin, Rebolo, & Zapatero-Osorio (1996) who noticed a similar trend comparing young red dwarfs of the Pleiades cluster to presumably older field M dwarfs. Previous M dwarf model atmospheres (Allard & Hauschildt 1995) did not show such a sensitivity due to the overestimated blocking caused by straight mean and JOLA opacities. To longer wavelengths an important veiling provided by the dust covers the 0.7 to 1.3 μm region in the high gravity model. Atomic lines and molecular bands are generally quite sensitive to gravity change in this range, while the near-infrared water vapor bands are also affected markedly (much more than in the grainless 2500K case discussed above). Especially, collision induced H_2 absorption cutting the flux in a negative slope at 2.2-2.3 μm, as well as the CO bands redwards of this, makes again the shape of the K band spectrum an excellent gravity indicator. A similar behavior is observed at 1500K (Figure 18), where however the dust is now so strong that most features, except H_2O band troughs, are no longer seen.

7.2. Comparing limits

Figures 19 and 20 compare the full-settling and full-dusty limits for $T_{\rm eff}$ = 2000 and 1500K respectively. In the 2000K case, the presence of dust opacities simply has the effect to veil the

optical to red spectral region, while the additional heat causes flux redistribution to the infrared. This T_{eff} and gravity is typical of dusty red and brown dwarfs. In the 1500K case however, the dust opacity profiles are blocking nearly all flux bluewards of 1.0 μm, and only the water vapor bands are still distinguishable in the AMES-Dusty model. The AMES-Cond models, on the other hand, are very transparent since all trace of TiO, VO, CaH, MgH and FeH have vanished through condensation to dust grains. And since more flux can escape from short wavelengths, the upper atmosphere is cooler and the water bands stronger.

As mentioned earlier, one of the most important effects of dust extinction in the photospheres of red and brown dwarfs is the resulting heating of the outer atmospheric layers. In Figure 7, we compare the thermal structures of our two limiting cases to NextGen models for two T_{eff}: one typical of M dwarfs and young/massive brown dwarfs (2800K), the other typical of the reddest L dwarfs (1800K). In the former case, the cloud layers form above the photosphere, as can be seen from Figure 1, such that heating takes place above the line forming region, leaving the thermal structure little affected by the dust. At 1800K, on the other hand, the clouds form deep into the photosphere (see Figure 2). The line forming region is therefore heated up by as much as 500K, while the internal layers only warm up by less than 80K. This effect is enough to dissociate water vapor by nearly 50% in the outer layers, leaving a far shallower structure over most of the photosphere. It is interesting to note that Cond models cooler than about T_{eff} = 1800K, have similar thermal structures than corresponding NextGen models.

This similarity of the thermal structures translates into similar synthetic spectra. We compare the present AMES-Cond models to our earlier brown dwarfs models (NextGen) as of Allard et al. (1996) in Figure 21 for the T_{eff} = 1000K case. Although the NextGen models used in our 1996 publication were constructed without dust condensation, the molecular bands of TiO, VO and FeH were completely crushed by the wings of the alkali lines and the results quasi independent of condensation. The models remain sensitive to the physics mainly in the inter-band regions at 1.0, 1.25, 1.6 and 2.2 μm which probe, by their relative brightness, the thermal structure of the atmosphere at various depths.

8. Colors

The models are most readily compared to large samples of stars and brown dwarfs in color-magnitude diagrams. The standard system of broadband colors is sufficiently constraining when evaluating the accuracy of the models. This is because most spectral features are several thousands of angstroems wide, and the remaining emission windows are well sampled by each bandpass: Z at 1.0 μm, J at 1.3 μm, H at 1.6 μm, K at 2.2 μm, M at 4.5 μm, and N at 10 μm. Methane bands appear in brown dwarfs cooler than about 1700K at 1.7, 2.4 and 3.3 μm, reducing the flux sampled by the H, K and L' bandpasses respectively. The pressure-induced H_2 opacity, on the other hand, depresses the flux in the K bandpass in the coolest brown dwarfs and low-metallicity dwarf stars.

We have computed synthetic $UBVRIJHKLL'M$ magnitudes by integrating our model spectra according to the photon count prescription at a wavelength step of 1Å. We have adopted the filter responses by Bessell & Brett (1988) and Bessell (1990), bringing our synthetic photometry on the Cousins and Johnson-Glass system. Transformations to the CIT or to other systems are readily obtained from Leggett (1992). As in previous papers, we used the energy distribution of Vega as observed by Hayes & Latham (1975); Hayes (1985) and Mountain et al. (1985) to provide an absolute calibration. Zero magnitudes and colors are assumed for Vega. The grainless NextGen models of Allard et al. (1996, 1997); Hauschildt, Allard, & Baron (1999); Baraffe et al. (1997, 1998), as well as the AMES-Cond and AMES-Dusty models from this work are compared to the observed stellar and brown dwarfs samples of Leggett (1992), Tinney (1993), Kirkpatrick & McCarthy (1994), Ianna & Fredrick (1995), Delfosse et al. (1997) and Zapatero Osorio, Martin, & Rebolo (1997) in Figure 22. Please note that we have applied here a +0.18 dex shift in $J-K$ to the current models to match the position of the NextGen models in the non-dusty regime in order to isolate the dust effects. This offset of the current models to the blue of the earlier NextGen models is due to some inaccuracies of the NASA-Ames H_2O opacity database in describing these relatively hot atmospheres (see Allard, Hauschildt and Schwenke 2000 for details).

These colors are interesting as they have helped distinguish interesting brown dwarf candidates from the databases of large scale surveys such as DENIS and 2MASS, and in obtaining an appreciation of the spectral sensitivity needed to detect new brown dwarfs. The methane bands cause the $J-K$ colors of brown dwarfs to get progressively bluer with decreasing mass and as they cool over time. Yet their $I-J$ colors remain very red which allows us to distinguish them from hotter low-mass stars, red shifted galaxies, red giant stars, and even from low metallicity brown dwarfs that are also blue due to pressure-induced H_2 opacities in the K bandpasses. Fortunately, grain formation and uncertainties in molecular opacities are far reduced under low metallicity conditions ([M/H]< -0.5). Therefore, model atmospheres of metal-poor subdwarf stars and halo brown dwarfs are free of uncertainties on the dust compared to their metal-rich counterparts. This has been nicely demonstrated by Baraffe et al. (1997) who reproduced closely the main sequences of globular clusters ranging in metallicities from [M/H]$= -2.0$ to -1.0, as well as the sequence of the Monet et al. (1992) halo subdwarfs in color-magnitude diagrams.

As can be seen from Figure 22, the AMES-Dusty models reproduce well the locus of the coolest dwarfs which deviate from that of main sequence stars red values of $J-K$ as dust effects grow in their atmospheres with decreasing effective temperature (see also Leggett et al 1998 for more such color comparisons). It appears, therefore, that this full-dusty limit where grain settling is negligible is adequate to reproduce the global properties of late-type low-mass stars and young or massive brown dwarfs with $T_{\rm eff} \leq 1800$K. Below this temperature, the AMES-Dusty models keeps getting redder and do not correspond to the properties of known T dwarfs illustrated in this diagram by the position of Gl229B and SDSS1624.

The locus of the AMES-Cond models for their part depends upon two major uncertainties. The first, likely tied to the second, is a hump of flux excess between 0.8 and 0.93 μm, i.e. in the

I-bandpass, which prevent the Cond models to become redder than $I - J = 4.2$. The second is the description of the far wings of the absorption lines of K I and Na I D as discussed above and illustrated in Figure 9. In Figure 22 we show two grids of Cond models: one computed with a coverage of the line wings opacity contributions of 5000Å on each side of each atomic line core (long dashed line), the other computed with a maximum coverage of 15000Å (short dashed line). Both grids use Lorentz profiles for the atomic lines. Obviously, the profile of the optical Na I D and K I doublets is no longer Lorenzian beyond 5000Å from the line cores as also been noted found by Burrows, Marley, & Sharp (2000). Since T dwarfs appear in the cone defined by these Cond models, an adequate theory of line broadening could be sufficient to reproduce their properties. Yet no theory exists for the treatment of the far wings of alkali elements broadened by collisions with H_2 and helium species to this date (Burrows, Marley, & Sharp 2000). Until these become available, the present grid with a line wing coverage of 5000Å seem to provide an acceptable compromise and limiting case (with the Dusty models) for the spectroscopic properties of brown dwarfs.

9. Discussion and Conclusions

We have investigated the two limiting cases of dust in low mass stars and brown dwarfs atmospheres by comparing two sets of models: 1) AMES-Cond with models ranging from $T_{\rm eff}$ = 3000 to 100K in 100K step, and with gravities ranging from $\log g = 2.5$ to 6.0 in steps of 0.5 dex at solar metallicity, and 2) AMES-Dusty with models from $T_{\rm eff} = 3000$ to 1400K in steps of 100K, with gravity ranging from $\log g = 3.5$ to 6.0 in steps of 0.5 dex. The AMES-Cond grid corresponds to the case where all dust has disappeared from the atmosphere by gravitational settling while the AMES-Dusty grid describes the case of negligible settling throughout the atmosphere. The two sets of models rely on the assumption that dust forms in equilibrium with the gas phase. See also Chabrier et al. (2000) for the corresponding evolution models of late type stars and brown dwarfs and a more detailed description of their photometric properties.

From the comparison of the two limits described here, and their comparisons to observations (see Section 8), we find that dwarfs with $T_{\rm eff} \geq 1800$K are successfully described by the full-dusty limit and conclude that dust must be in close equilibrium with the gas phase with little sedimentation, or compensated sedimentation effects. This would be the case if, for example, convective mixing was efficient in returning material to the line forming regions. We are exploring these issue by modeling, hydrodynamically, the convection in 3D models (Ludwig et al 2000, in preparation).

Observations of T dwarfs such as Gliese 229B indicate that brown dwarfs with $T_{\rm eff} \leq 1300$K are, on the other hand, more closely following the full-settling limiting case as has been shown also by Tsuji, Ohnaka, & Aoki (1996); Tsuji et al. (1996); Allard et al. (1996) and Marley et al. (1996). However there has been a history of failure to explain the optical spectra of these cool brown dwarfs since the discovery of Gl229B. For example, Griffith et al. (1998) claimed a veiling due to photo-dissociation by the parent starlight in the upper brown dwarf atmosphere. But this

suggestion did not pass the acid test, and free-floating T dwarfs were discovered (Tsvetanov et al. 2000). Finally, Tinney et al. (1998); Kirkpatrick et al. (1999a); Burrows, Marley, & Sharp (2000) and Liebert et al. (2000) have stressed the importance of the λ5891,5897Å Na I D and λ7687,7701Å K I resonance doublets. Our analysis recover the latter results in predicting the red wings of these lines to heat up the photospheric thermal structure by as much as 100K, and to define the pseudo-continuum out to at least 1.1 μm in T dwarfs. This indicates that red flux out to 1.1 μm must be sensitive to gravity. We also find that the traditional Lorentz profile does not describe adequately their red wings, beyond 5000Å from the line center: it overestimate the wing opacity contribution. While this overestimation has negligible effects on the thermal structure as long as the lines are included in the calculation, it is important to realize that an adequate handling of the collisional broadening of alkali lines by H_2 and He must be developed in order to model successfully the optical to 1.1 μm flux and VRI colors of T dwarfs (Burrows, Marley, & Sharp 2000). Nevertheless we believe that our AMES-Cond models, limited in the coveraged of the atomic line wings contributions, can provide the full-settling limit that they were intended to define.

Based on the Cond models, we also find that currently known T dwarfs with effective temperatures around 1000K are in a special regime where several of their important spectral features start to reverse their behavior with decreasing T_{eff}: Cs I lines weaken as Cs begins to lock into CsCl, and CO and NH3 bands begin to grow in strength as a result of decreasing background opacities. While Noll, Geballe & Marley (1997), Griffith & Yelle (2000), and Saumon et al. (2000) all fail to reproduce these features in Gl229B with solar composition models in thermodynamic equilibrium, it is perhaps due to the fact that each of these spectral synthesis analysis were based upon thermal structures exempt of atomic line opacities? Indeed, in the fit to the overall spectrum, a sub-solar composition could compensate (via an increased pressure) for the neglect of atomic line opacities in the thermal structure calculations. To clarify the issue of the metallicity of Gl229B, we need to explore the composition of the parent star Gl229A. This work is in progress and will be published shortly. However, we feel that it is unlikely, though not impossible, that the first known T dwarfs be metal-deficient, while more massive brown dwarfs are only found in metal-rich environments.

There remains a regime between 1300 and 1800K where brown dwarfs should behave between these limits. We hope that our two sets of models can help bracket brown dwarf's properties and identify objects. They can also be used to evaluate the effects of intrinsic variability as weathering effects that cause clouds to form and vanish. The full-dusty models give the aspect of a cloudy atmosphere while the Cond models resemble a cloud-free sky.

In the atmospheres of brown dwarfs and late-type M dwarfs, the dust likely forms in clouds distributed more or less evenly across the dwarf's surface as we observe on planets. These cloud layers should be well-confined close to the deepest/hottest level where the grain-type can condense (Lunine et al. 1989; Tsuji, Ohnaka, & Aoki 1999; Ackerman & Marley 2000, see for example). But the physical process that defines this confinement of the cloud layers are not known. It could either be: i)an inefficient condensation of the dust in the upper atmosphere, or ii) an efficient gravitational

settling (sedimentation) of the dust in those upper layers. Time-dependent grain growth analysis must be done to determine the first. This work is under progress at the Berlin University. But our CE calculations indicate that the local [T,P] conditions favor dust formation. The second can be understood by opposing sedimentation and convective mixing, one pushing the grains down, the other bringing upwards material to condense. Since the convection zone retreats progressively from the photosphere with decreasing $T_{\rm eff}$, it seems to be a natural explanation of the fact that dust also retreats from the photosphere as $T_{\rm eff}$ decreases. This is why we mention the potential importance of gravitational settling throughout this paper.

The Cond models represent a limiting case where these cloud layers are all sitting below the photosphere, independently of the cause for the cloud confinement. The Dusty models on the other hand represent a case where confinement does not occur. So it is clear that nature is likely between the Cond and Dusty limits, with partial gravitational settling occurring with a fraction that varies with depth in the atmosphere, the detailed modeling of this process relies on characteristic diffusion time scales for several processes such as condensation, sedimentation, coagulation and convective mixing to name a few which are not known accurately for the type of grains important under the conditions prevailing in brown dwarf atmospheres. Models incorporating these effects can therefore only be exploratory. The two limits described here will remain useful until the physics of these processes become solidly mastered.

All the models discussed in this paper are available upon request. We will also provide, as we have in the past, colors computed from these spectra on any requested color system. Please send requests to France Allard and consult the CRAL anonymous ftp site.

We wish to thank specially Richard Freedman (NASA-Ames) for joining us in the analysis of the VO and CrH line formation in M dwarfs and brown dwarfs, Hans G. Ludwig (Lund) for a lot of very instructive discussions and for his interest in dust formation in brown dwarfs, and Tristan Guillot (Obsv. de Nice) for his support and interesting collaborations to come. We thank also Gilles Chabrier, Isabelle Baraffe and Travis Barman for proofreading and providing some orientation to the draft. This research is supported by CNRS as well as NASA LTSA NAG5-3435 and a NASA EPSCoR grant to Wichita State University. Peter Hauschildt and Andreas Schweitzer acknowledge support in part from NASA ATP grant NAG 5-3018, NAG 5-8425 and LTSA grant NAG 5-3619 to the University of Georgia. Some of the calculations presented in this paper were performed on the IBM SP2 of the CINES, and the UGA UCNS at the San Diego Supercomputer Center (SDSC) and the Cornell Theory Center (CTC), with support from the National Science Foundation. We thank all these institutions for a generous allocation of computer time.

REFERENCES

Ackerman, A., & Marley, M. 2000, ApJ, submitted.

Alexander, D. R. 1975, ApJS, 29, 363.

Alexander, D. R., & Ferguson, A. J. 1994, ApJ, 437, 879.

Alexander, D. R., Ferguson, A. J., Tamanai, A., Allard, F., Hauschildt, P. H. & Vukovich, J. G. 2000, ApJ, in prep.

Alexander, D. R., Johnson, H. R., & Rypma, R. L. 1983, ApJ, 272, 773.

Allard, F. 1990, *Model Atmospheres for M-Dwarfs*, Ph.D. thesis, University of Heidelberg.

—. 1995, Nature, 378, 441.

—. 1998, "Model Atmospheres: Brown Dwarfs from the Stellar Perspective (invited review)", In *ASP Conf. Ser. 134: Brown Dwarfs and Extrasolar Planets*, page 370.

Allard, F., & Hauschildt, P. H. 1995, ApJ, 445, 433.

Allard, F., Hauschildt, P. H., Baraffe, I., & Chabrier, G. 1996, ApJ, 465, L123.

Allard, F., Hauschildt, P. H., Alexander, D. R., & Starrfield, S. 1997, ARA&A, 35, 137.

Allard, F., Alexander, D. R., & Hauschildt, P. H. 1998, "Model Atmospheres of Very Low Mass Stars and Brown Dwarfs", In *ASP Conf. Ser. 154: Tenth Cambridge Workshop on Cool Stars, Stellar Systems, and the Sun*, volume 10, page 63.

Allard, F., Alexander, D. R., Tamanai, A., & Hauschildt, P. H. 1998, "Photospheric Dust Grain Formation in Brown Dwarfs", In *ASP Conf. Ser. 134: Brown Dwarfs and Extrasolar Planets*, page 438.

Allard, F., Hauschildt, P. H., & Schwenke, D. W. 2000a, ApJ, 540, 1005.

Bailer-Jones, C. A. L., & Mundt, R., 2001, A&A, 367, 218.

Baraffe, I., Chabrier, G., Allard, F., & Hauschildt, P. H. 1995, ApJ, 446, L35.

—. 1997, A&A, 327, 1054.

—. 1998, A&A, 337, 403.

Baron, E., Hauschildt, P. H., Branch, D., Wagner, R.M., Austin, S.J., Filippenko, A.V., & Matheson, T. 1993, ApJ, 416, L21.

Chabrier, G., Baraffe, I., Allard, F., & Hauschildt, P. H. 2000, ApJ, 542, 464.

Barman, T. S., Hauschildt, P. H., & Allard, F. 2000, ApJ, submitted.

Basri, G., Marcy, G., & Graham, J. R. 1996, ApJ, 458, 600.

Basri, G., Mohanty, S., Allard, F., Hauschildt, P. H., Delfosse, X., Martín, E. L., Forveille, T., & Goldman, B. 2000, ApJ, 538, 363–385.

Becklin, E. E., & Zuckerman, B. 1988, Nature, 336, 656–658.

Begemann, B., Dorschner, J., Henning, Th., Mutschke, H., & Nass, R. 1997, ApJ, 476, 199.

Bessell, M. S. 1990, PASP, 102, 1181.

Bessell, M. S., & Brett, J. M. 1988, PASP, 100, 1134.

Bohren, C. F., & Huffman, D. R. 1983, *Absorption and Scattering of Light by Small Particles*, page 82, John Wiley & Sons, New York.

Borysow, A., & Frommhold, L. 1986a, ApJ, 311, 1043.

—. 1986b, ApJ, 303, 495.

—. 1986c, ApJ, 304, 849.

—. 1987a, A&A, 320, 437.

—. 1987b, ApJ, 318, 940.

Borysow, A., & Tang 1993, Icarus, 105, 175.

Borysow, A., Jorgensen, U. G., & Cheng 1997a, A&A, 324, 185.

—. 1997b, A&A, 324, 185.

Burrows, A., & Sharp, C. M. 1999, ApJ, 512, 843–863.

Burrows, A., Hubbard, W. B., Saumon, D., & Lunine, J. I. 1993, ApJ, 406, 158–171.

Burrows, A., Marley, M., Hubbard, W. B., Lunine, J. I., Guillot, T., Saumon, D., Freedman, R., Sudarsky, D., & Sharp, C. 1997, ApJ, 491, 856.

Burrows, A., Marley, M. S., & Sharp, C. M. 2000, ApJ, 531, 438–446.

Cameron, A. G. W., & Pine, M. R. 1973, Icarus, 18, 377.

Guillot, T., Gautier, D., Chabrier, G. & Morel, B. 1994, Icarus, 112, 354.

Chase, M. W., Davis, C. A., Downey, J. R., Frurip, D. J., McDonald, R. A., & Syverud, A. N. 1985, J. Phys. Chem. Ref. Data, 14, Sup.1.

Delfosse, X., Tinney, C. G., Forveille, T., Epchtein, N., Bertin, E., Borsenberger, J., Copet, E., De Batz, B., Fouque, P., Kimeswenger, S., Le Bertre, T., Lacombe, F., Rouan, D., & Tiphene., D. 1997, A&A, 327, L25–L28.

Dorschner, J., Begemann, B., Henning, Th., Jager, C., & Mutschke, H. 1995, A&A, 300, 503.

Goorvitch, D. 1994, ApJS, 95, 535.

Goorvitch, D., & Chackerian, C. J. 1994a, ApJS, 91, 483.

—. 1994b, ApJS, 92, 311.

Grevesse, N., & Noels, A. 1993, In *Origin and Evolution of the Elements*, N. Prantos, E. Vangioni-Flam, and M. Casse, editors, Cambridge University Press, page p.14.

Griffith, C. A. & Yelle, R. V. 2000, Science, 282, 2063.

Griffith, C. A., Yelle, R. V. & Marley, M. S. 1998, Science, 282, 2063.

Grossman, L. 1972, Geochemica et Cosmochimica Acta, 36, 597.

Gruszka, M., & Borysow, A. 1997, Icarus, 129, 172.

Gurvich, L., & Glushko, V. 1982, Thermodinamicheskie Svoistva Individual'nikh Veschev, 4 (Moscow: Sovit Acad. Sci.).

Hauschildt, P. H. 1992, JQSRT, 47, 433.

Hauschildt, P. H., Allard, F., Alexander, D. R. & Baron, E. 1997, ApJ, 488, 428.

Hauschildt, P. H., Allard, F., & Baron, E. 1999, ApJ, 512, 377.

Hauschildt, P. H., & Baron, E. 1999, Journal of Computational and Applied Mathematics, 102, 41–63.

Hayes, D. S. 1985, In *Calibration of Fundamental Stellar Quantities*, I.A.U. Colloquium 11, page 225.

Hayes, D. S., & Latham, D. W. 1975, ApJ, 197, 593.

Husson, N., Bonnet, B., Scott, N. A., & Chedin, A. 1992, JQSRT, 48, 509.

Ianna, P. A., & Fredrick, L. W. 1995, ApJ, 441, L47–L50.

Irwin, A. W. 1988, A&A Supp., 74, 145.

Jørgensen, U. G. 1994, A&A, 284, 179.

Kirkpatrick, J. D., & McCarthy, Donald W., J. 1994, AJ, 107, 333–349.

Kirkpatrick, J. D., Allard, F., Bida, T., Zuckerman, B., Becklin, E. E., Chabrier, G., & Baraffe, I. 1999a, ApJ, 519, 834–843.

Kirkpatrick, J. D., Reid, I. N., Liebert, J., Cutri, R. M., Nelson, B., Beichman, C. A., Dahn, C. C., Monet, D. G., Gizis, J. E., & Skrutskie, M. F. 1999b, ApJ, 519, 802–833.

Kurucz, R. L. 1993, Molecular data for opacity calculations, Kurucz CD-ROM No. 15.

Kurucz, R. L. 1994, Atomic data for opacity calculations, Kurucz CD-ROM No. 1.

Koike, C., Kaito, C., Yamamato, T., Shibai, H., Kimura, S., & Suto, H. 1995, Icarus, 114, 203.

Leggett, S. K. 1992, ApJS, 82, 351.

Leggett, S. K., Allard, F., Berriman, G., Dahn, C. C., & Hauschildt, P. H. 1996, ApJS, 104, 117.

Leggett, S. K., Allard, F., & Hauschildt, P. H. 1998, ApJ, 509, 836–847.

Leggett, S. K., Allard, F., & Hauschildt, P. H. 1998, ApJ, 509, 836.

Leggett, S. K., Allard, F., Dahn, C., Hauschildt, P. H., Kerr, T. H., & Rayner, J. 2000, ApJ, 535, 965–974.

Leinert, C., Allard, F., Richichi, A., & Hauschildt, P. H. 1999, A&A, 353, 691.

Liebert, J., Reid, I. N., Burrows, A., Burgasser, A. J., Kirkpatrick, J. D., & Gizis, J. E. 2000, ApJ, 533, L155.

Lodders, K. 1999, ApJ, 519, 793.

Lodders, K. & Fegley, B. Jr. 1998, Meteor. & Planetary Sci., 33, 871.

Lunine, J. I., Hubbard, W. B., Burrows, A., Wang, Y.-P. & Garlow, K., 1989, ApJ, 338, 314.

Marley, M., Saumon, D., Guillot, T., Freedman, R., Hubbard, W. B., Burrows, A., & Lunine, J. I. 1996, Science, 272, 1919.

Martin, E. L., Rebolo, R., & Zapatero-Osorio, M. R. 1996, ApJ, 469, 706.

Martín, E. L., Basri, G., Brandner, W., Bouvier, J., Zapatero Osorio, M. R., Rebolo, R., Stauffer, J., Allard, F., Baraffe, I., & Hodgkin, S. T. 1998, ApJ, 509, L113–L116.

Monet, D. G., Dahn, C. C., Vrba, F. J., Harris, H. C., Pier, J. R., Luginbuhl, C. B., & Ables, H. D. 1992, AJ, 103, 638.

Mountain, C. M., Leggett, S. K., Selby, M. J., Blackwell, D. E., & Petford, A. D. 1985, A&A, 151, 399.

Nakajima, T., Oppenheimer, B. R., Kulkarni, S. R., Golimowski, D. A., Matthews, K., & Durrance, S. T. 1995, Nature, 378, 463.

Neale, L., & Tennyson, J. 1995, ApJ, 454, L169.

Neale, L., Miller, S., & Tennyson, J. 1996, ApJ, 464, 516.

Noll, K. S., Geballe, T. R., & Marley, M. S. 1997, ApJ, 489, L87.

Oppenheimer, B. R., Kulkarni, S. R., Matthews, K., & Nakajima, T. 1995, Science, 270, 1478.

Partridge, H., & Schwenke, D. W. 1997, J. Chem. Phys., 106, 4618.

Phillips, J. G., & Davis, S. P. 1993, ApJ, 409, 860.

Pollack, J. B., McKay, C. P., & Christofferson, B. M. 1985, Icarus, 64, 471.

Rebolo, R., Martin, E., & Magazzù, A. 1992, ApJ, 389, L83.

Rebolo, R., Martin, E. L., Basri, G., Marcy, G. W., & Zapatero-Osorio, M. R. 1996, ApJ, 469, L53.

Rothman, L. S., Gamache, R. R., Tipping, R. H., Rinsland, C. P., Smith, M. A. H., Chris Benner, D., Malathy Devi, V., Flaub, J.-M., Camy-Peyret, C., Perrin, A., Goldman, A., Massie, S. T., Brown, L., & Toth, R. A. 1992, JQSRT, 48, 469.

Ruiz, M. T., Leggett, S. K., & Allard, F. 1997b, ApJ, 491, L107.

Samuelson, R. E., Nath, N., & Borysow, A. 1997, Planetary & Space Sciences, 45/8, 959.

Saumon, D., Bergeron, P., Lunine, J. I., Hubbard, W. B., & Burrows, A. 1994, ApJ, 424, 333–344.

Saumon, D., Geballe, T. R., Leggett, S. K., Marley, M. S., Freedman, R. S., Lodders, K., Fegley, B., Jr., Sengupta, S. K. 2000, ApJ, 541, 374.

Schryber, H., Miller, S., & Tennyson, J. 1995, JQSRT, 53, 373.

Schweitzer, A., Hauschildt, P. H., Allard, F., & Basri, G. 1996, MNRAS, 283, 821.

Schweitzer, A., Gizis, J. E., Hauschildt, P. H., Allard, F., & Reid, I. N. 2000, ApJ, submitted.

Schwenke, D. W. 1998, Chemistry and Physics of Molecules and Grains in Space. Faraday Discussion, 109, 321.

Sharp, C. M., & Huebner, W. F. 1990, ApJS, 72, 417–431.

Strauss, M. A., Fan, X., Gunn, J. E., Leggett, S. K., Geballe, T. R., Pier, J. R., Lupton, R. H., Knapp, G. R., Annis, J., Brinkmann, J., Crocker, J. H., Csabai, I. ., Fukugita, M., Golimowski, D. A., Harris, F. H., Hennessy, G. S., Hindsley, R. B., Ivezić , Z., Kent, S., Lamb, D. Q., Munn, J. A., Newberg, H. J., Rechenmacher, R., Schneider, D. P., Smith, J. A., Stoughton, C., Tucker, D. L., Waddell, P., & York, D. G. 1999, ApJ, 522, L61–L64.

Tinney, C. G. 1993, ApJ, 414, 279–301.

Tinney, C. G., Delfosse, X., Forveille, T., & Allard, F. 1998, A&A, 338, 1066–1072.

Tropf, W. J. & Thomas M. E. 1990, *Handbook of Optical Constants of Solids II*,E.D. Palik (ed), Orlando, Fl., Academic Press, Inc., page 883.

Tsuji, T. 1973, A&A, 23, 411.

—. 1995, In *The Bottom of the Main Sequence - and Beyond*, C. Tinney, editor, ESO Astrophysics Symposia, page 45, Springer-Verlag Berlin Heidelberg.

Tsuji, T.; Ohnaka, K.; Aoki, W. 1999, ApJ, 520, L119.

Tsuji, T., Ohnaka, K., Aoki, W., & Makajima, T. 1996, ApJ, 308, L29.

Tsuji, T., Ohnaka, K., & Aoki, W. 1996, A&A Letters, 305, L1.

Tsvetanov, Z. I., Golimowski, D. A., Zheng, W., Geballe, T. R., Leggett, S. K., Ford, H. C., Davidsen, A. F., Uomoto, A., Fan, X., Knapp, G. R., Strauss, M. A., Brinkmann, J., Lamb, D. Q., Newberg, H. J., Rechenmacher, R., Schneider, D. P., York, D. G., Lupton, R. H., Pier, J. R., Annis, J., Csabai, I. ., Hindsley, R. B., Ivesić, Z., Munn, J. A., Thakar, A. R., & Waddell, P. 2000, ApJ, 531, L61–L65.

Zapatero Osorio, M. R., Martin, E. L., & Rebolo, R. 1997, A&A, 323, 105–112.

Zapatero Osorio, M. R., Rebolo, R., Martin, E. L., Basri, G., Magazzu, A., Hodgkin, S. T., Jameson, R. F., & Cossburn, M. R. 1997, ApJ, 491, L81.

Figure captions

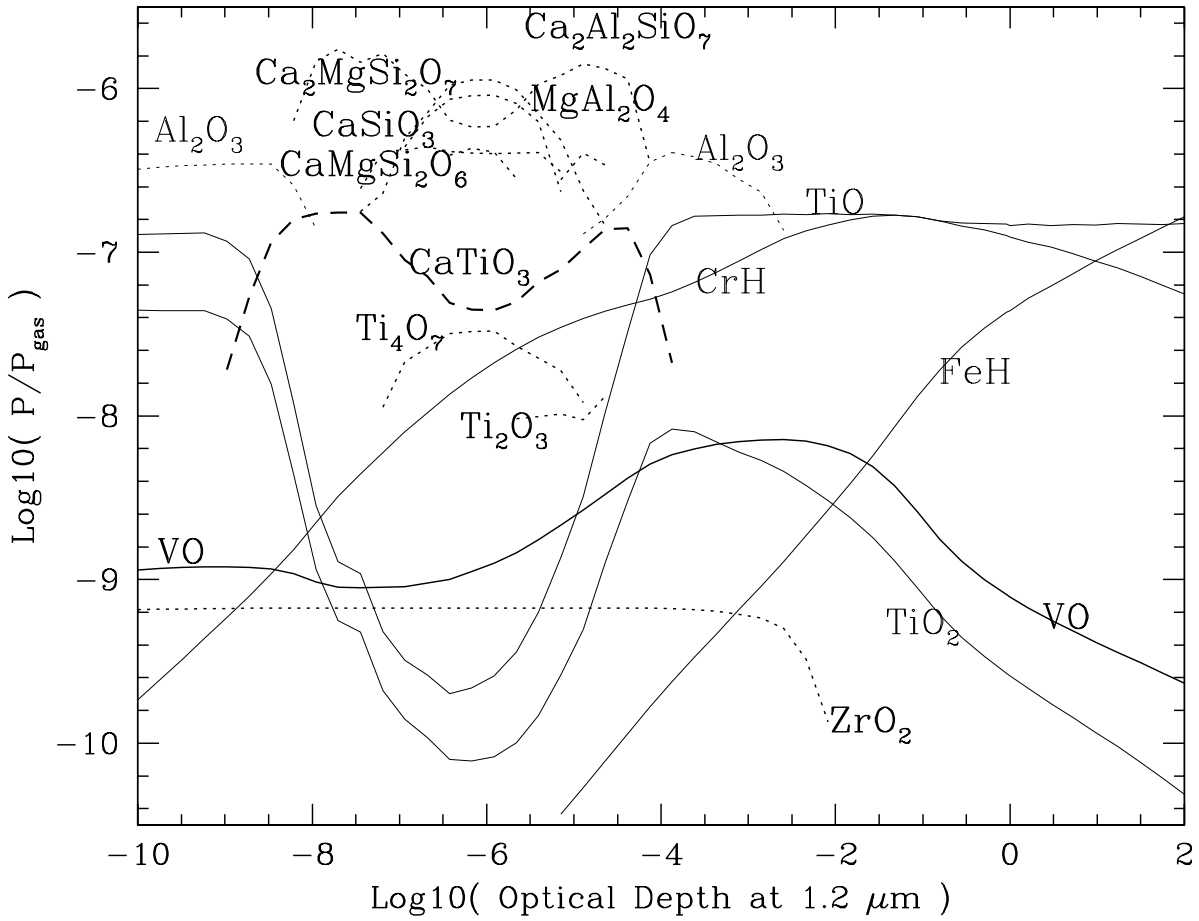

Fig. 1.— Run of the relative abundances of gas phase (full lines) and crystallized species across a T_{eff} = 2600 K model atmosphere typical of the young Pleiades brown dwarfs Teide1 and Calar3. The condensation of perovskite ($CaTiO_3$, dashed line) is the principle cause of TiO depletion in the atmospheres of dwarfs later than about M6. The abundance of the condensate Ca_2SiO_4 is drawn at log10(τ)= −5.0 but is not labeled for sake of clarity.

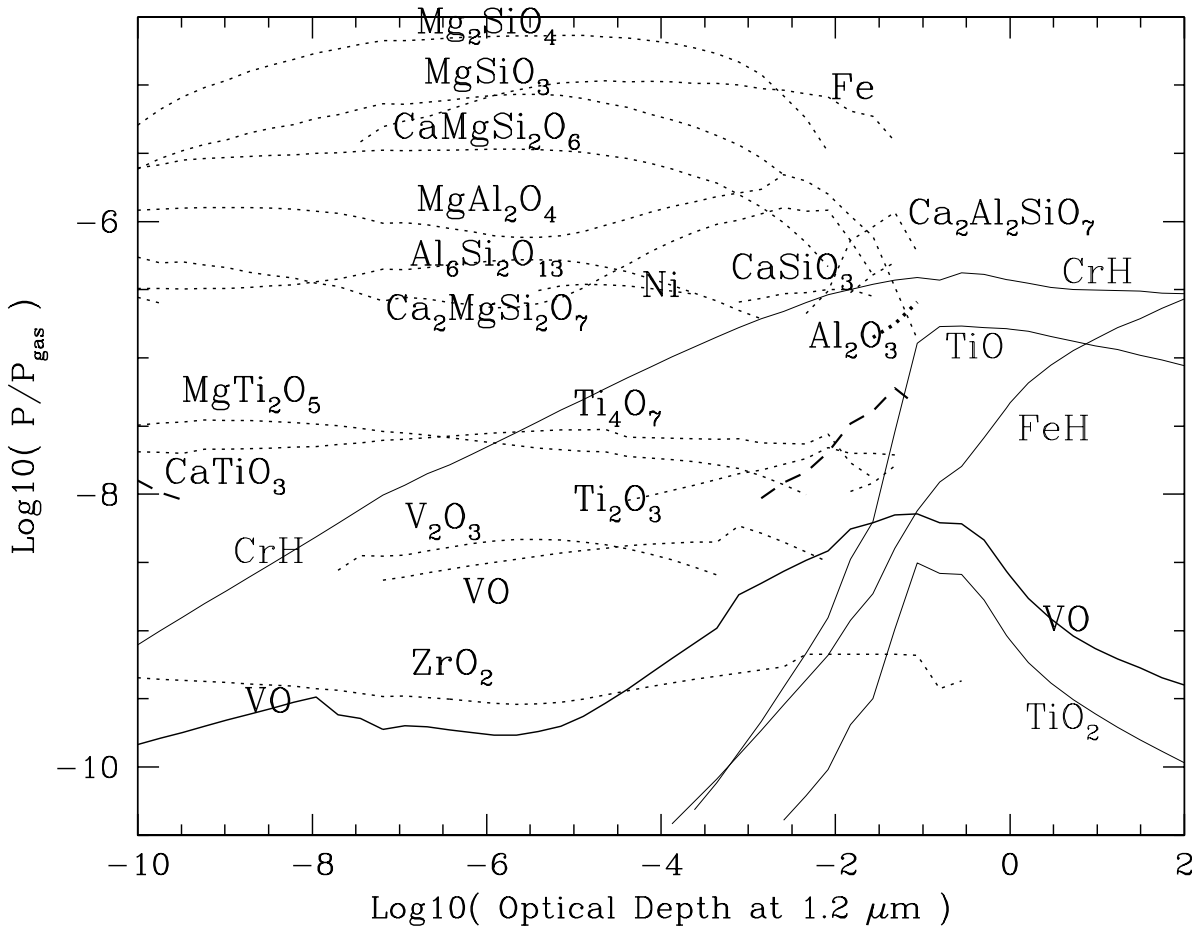

Fig. 2.— Same as above for a T_{eff} = 1800 K model atmosphere typical of the reddest known field dwarfs GD165B, Kelu1, and the DENIS objects.

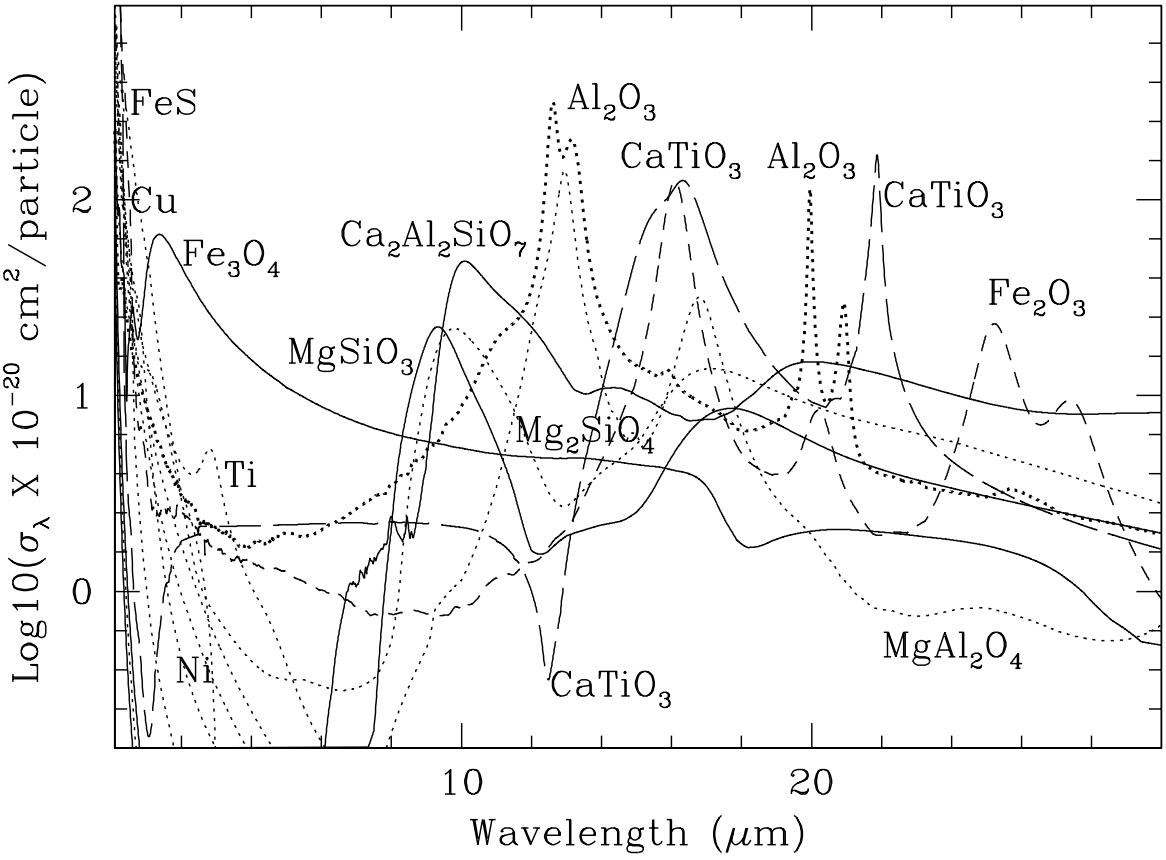

Fig. 3.— The extinction cross-sections per particle of dust grains. The mie formalism is used assuming a power-law ($\alpha = -3.5$) grain size distribution with diameters from 0.00625 and 0.24 μm. Monoatomic grains such as Fe, Cu, and Ni contribute scattering at optical wavelengths only, while corundum, magnesium aluminium spinel, calcium titenide, hematite, magnetite, and $Ca_2Al_2SiO_7$ crystals show strong peaks of absortion, at infrared wavelengths, that could compete with the local water vapor "continuum" in hot/young brown dwarfs. Note however that if the grains were elliptical and randomly oriented, the sharp absorption peaks shown here could be washed out.

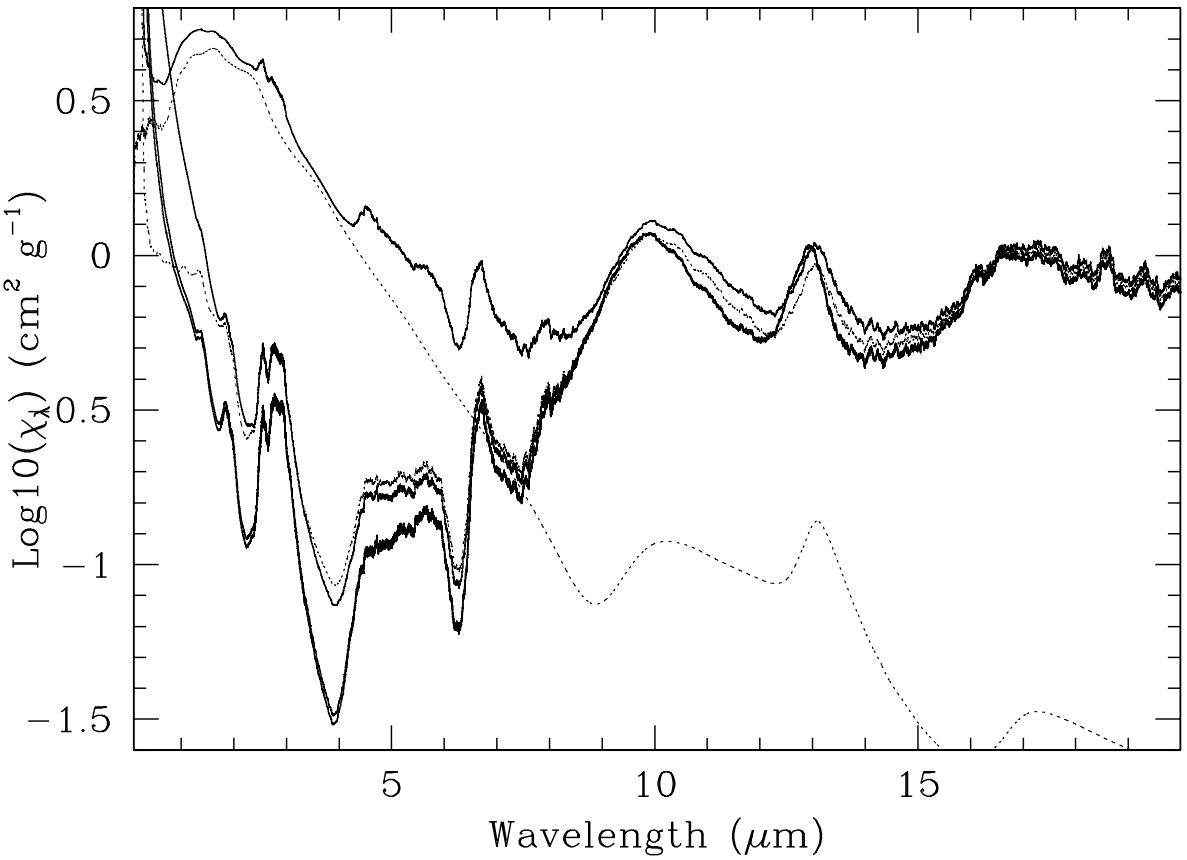

Fig. 4.— The extinction profiles are compared for grain size distributions with 1, 2, 10 and 100 times the ISM values adopted for this work (full lines from bottom to top respectively, where the two first curves are nearly undistinguishable). The scattering and absorption contributions of the 100 ISM profile are also shown (dotted lines). The conditions are those of the photospheric layers ($\tau_{1.2\mu m} \approx 10^{-4}$, i.e. T$\approx$ 1300K) of our standard 1800K AMES-Dusty model atmosphere. The structures seen in the profile at $\lambda > 8.5\mu$m are due to dust absorption (Mg_2SiO_4 at 10 and 16.5 μm and $MgAl_2O_4$ at 13 μm). Scattering contributions dominate below 0.5μm, and remain modest at longer wavelengths for grain sizes $\leq$ 10 times the adopted values. The absoption profile, on the other hand, is only little sensitive to grain sizes.

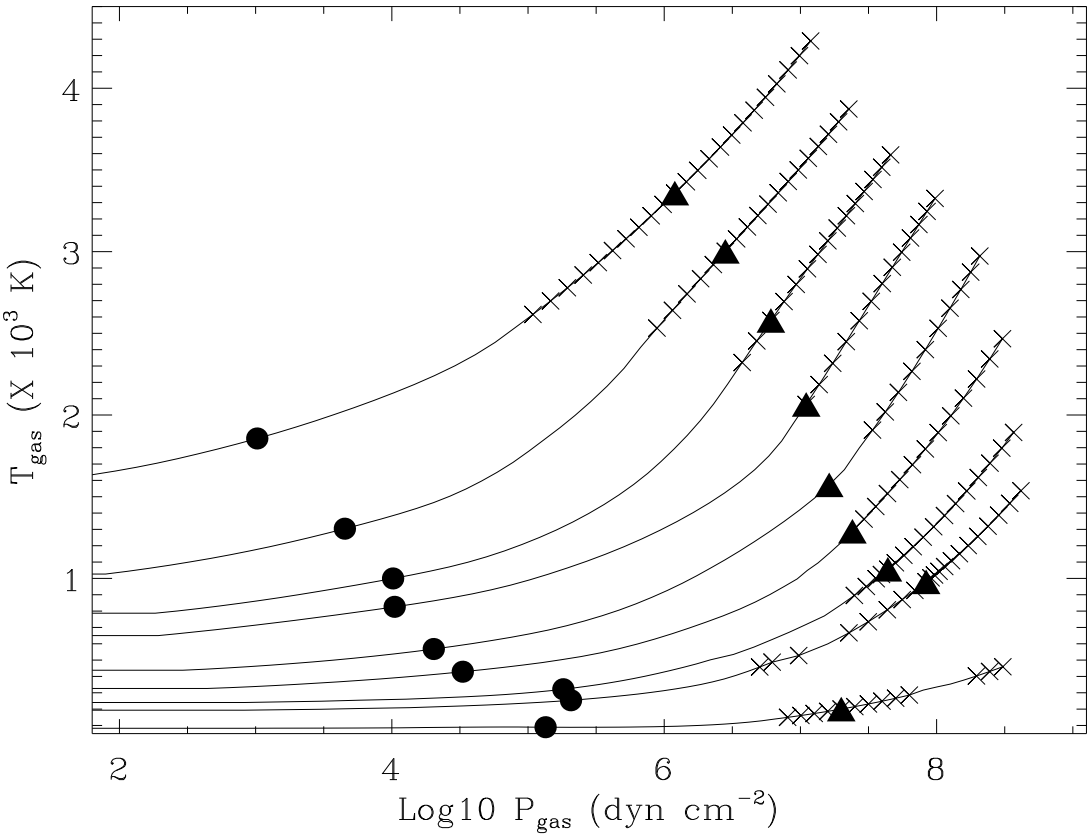

Fig. 5.— Thermal structures of the AMES-Cond models with T_{eff} ranging from 3000 to 100K by steps of 500K, with two additional models at 700 and 400K, logg=5.0, and solar metallicity. The convection zones are labeled with cross-symbols. The approximate location of the photosphere is indicated with filled circles and triangles marking the $\tau_{1.2\mu m} = 10^{-4}$ and 1.0 optical depths. All models shown stop at $\tau_{1.2\mu m} = 10$. As T_{eff} decreases, the photosphere becomes progressively more isothermal.

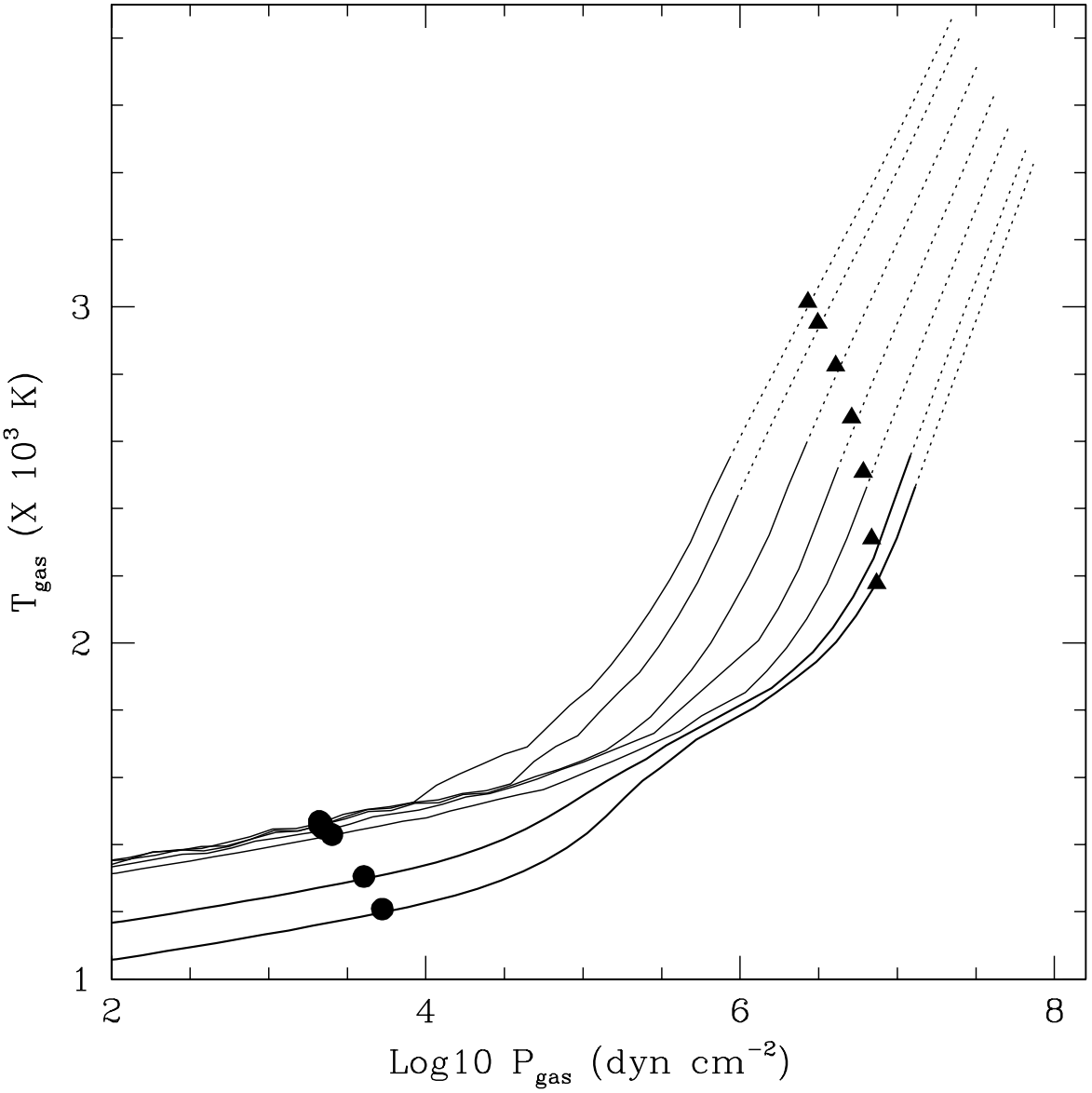

Fig. 6.— Thermal structures of the fully dusty models with $T_{\rm eff}$ ranging from 2400 to 1600K by steps of 200K, with two additional models at 2500 and 1500K, logg=5.0. None of the curves shown actually overcross. The radiative zones are marked by full lines while the convective region is shown as dotted lines. The location of the photosphere is also indicated, with full circles and triangles marking the $\tau_{1.2\mu\rm m} = 10^{-4}$ and 1.0 optical depths respectively. The strongest optical molecular bands and resonance lines form near $\tau_{1.2\mu\rm m} = 10^{-4}$. All models shown stop at $\tau_{1.2\mu\rm m} = 10$.

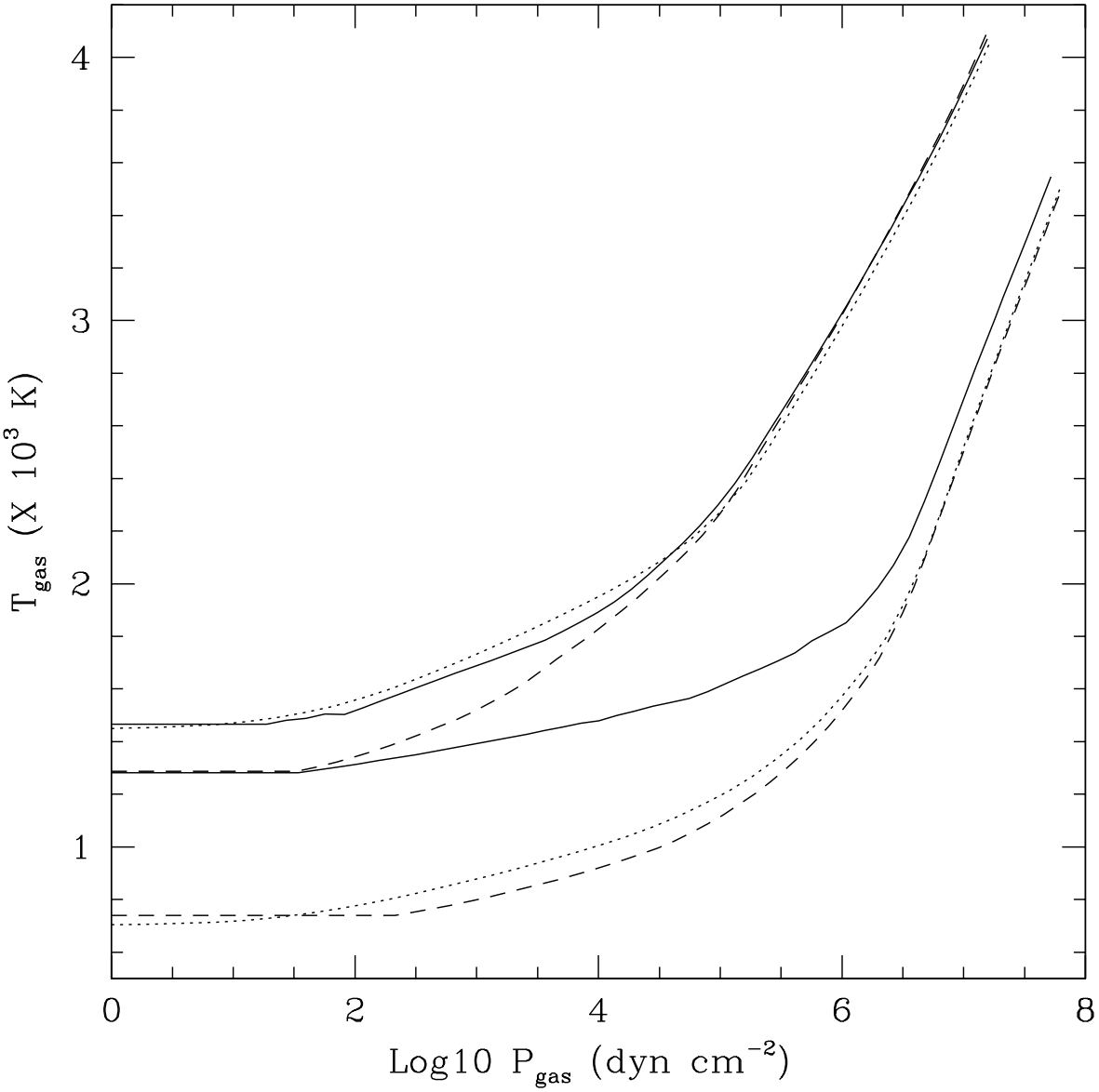

Fig. 7.— Thermal structures of models with T_{eff} = 2800K and 1800K, logg=5.0, and solar metallicity for three types of models: (1) the standard NextGen models treated in gas phase only (dotted line); (2) the AMES-Dusty models assuming a full distribution of the dust (full line), and; (3) the AMES-Cond models including dust in the CE but ignoring their opacities (dashed line). All models are converged. Note that the NextGen models use a different source of water vapor opacity (see text).

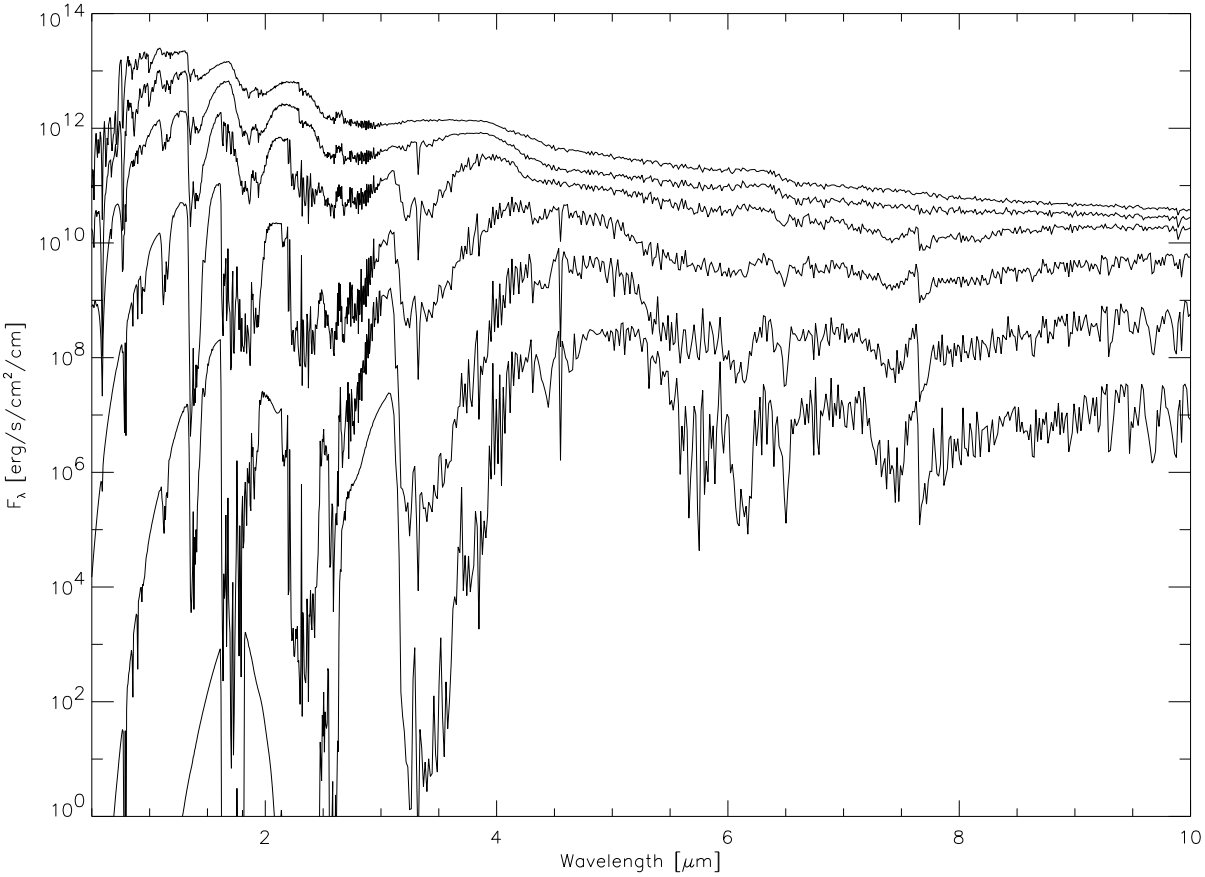

Fig. 8.— Spectral sequence of brown dwarfs to EGP model atmospheres in the total settling (AMES-Cond) approximation. From top to bottom: $T_{\rm eff} = 2500, 1900, 1300, 700, 400$K, and 200K. The gravity is fixed to $\log g = 5.0$. These models (AMES-Cond) assume complete settling of the grains (i.e. neglects all dust opacity). The spectral resolution has been reduced from 2Å to 30Å by boxcar smoothing in order to make comparison of the spectra easier. We observe that CH_4 bands already develop at 2000K in these extremely transparent and cool AMES-Cond atmospheres. They gradually replace water vapor bands while H_2O condenses to ice below 300K.

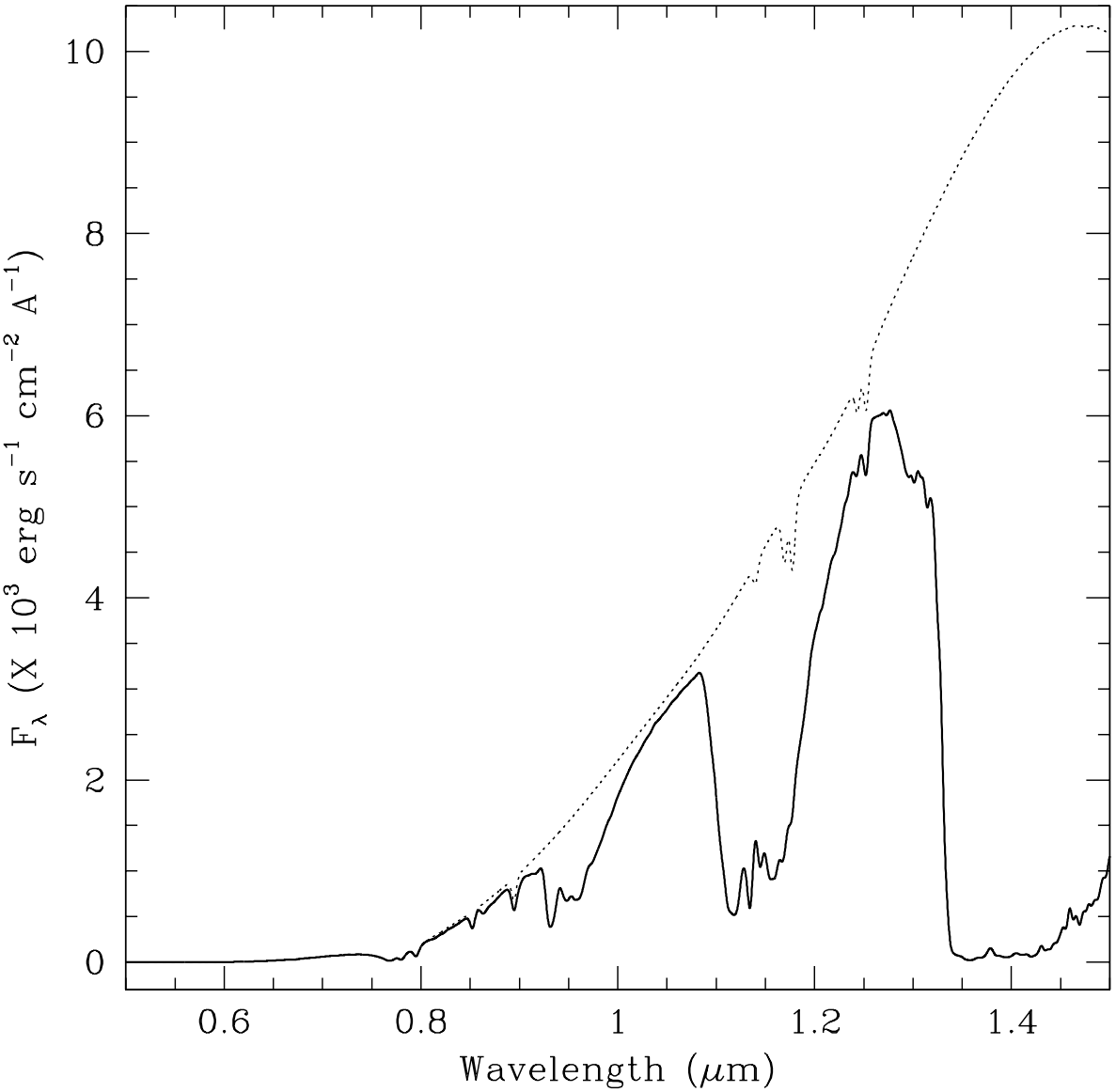

Fig. 9.— To isolate atomic features we compare a T_{eff} = 1000K AMES-Cond model (full line) with a spectrum obtained by neglecting all molecular lines (dotted lines). The pseudo-continuum is essentially formed by the van der Waals wings of the Na I D and K I resonance doublets at λ5891,5897Å and λ7687,7701Å. Weaker lines of Rb I (λ7802 and 7949Å), Cs I (λ8523 and 8946Å), and K I (λ11693,11776 and λ12436,12525Å) are also seen. The background flux (obtained by neglecting both atomic and molecular lines, not shown) lies outside the plot! The spectral resolution is reduced to 30Å for this illustration.

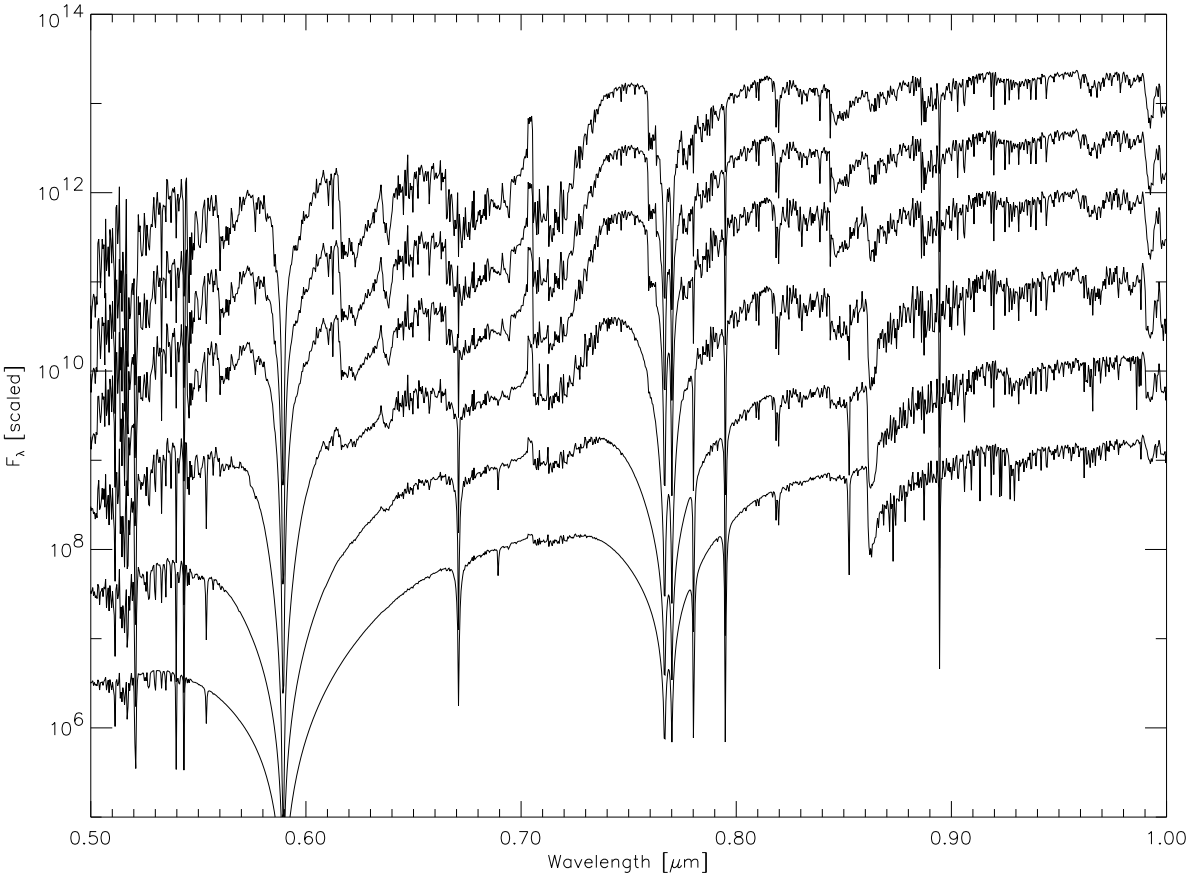

Fig. 10.— Same as Figure 8 in the optical to near-red spectral range. Here the spectra have been arbitrarily scaled to facilitate the comparison. From top to bottom: $T_{\rm eff}$ = 2500, 2400, 2300, 2000, 1700, and 1500K. The spectral resolution is 2Å.

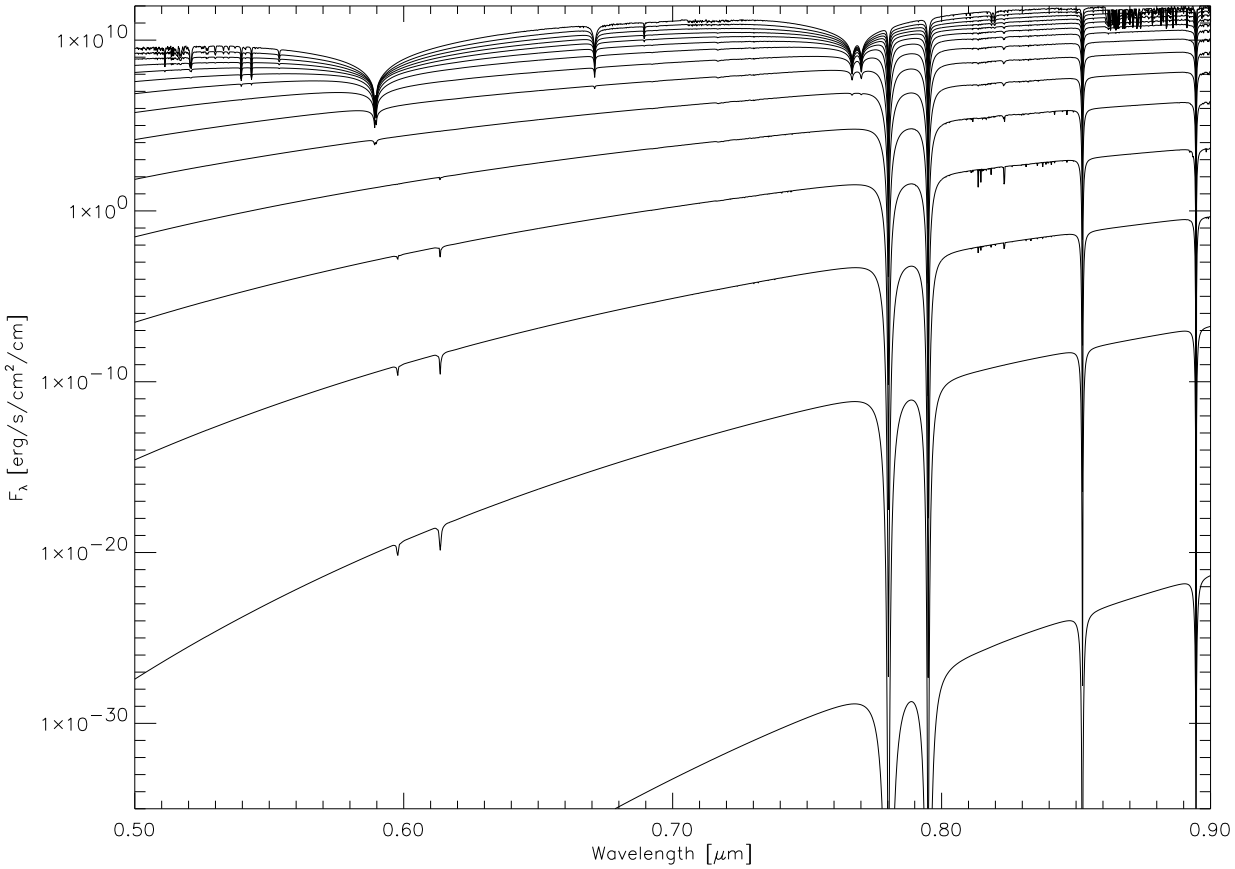

Fig. 11.— Same as Figure 10 for models from 1500K to 100K at 100K steps.

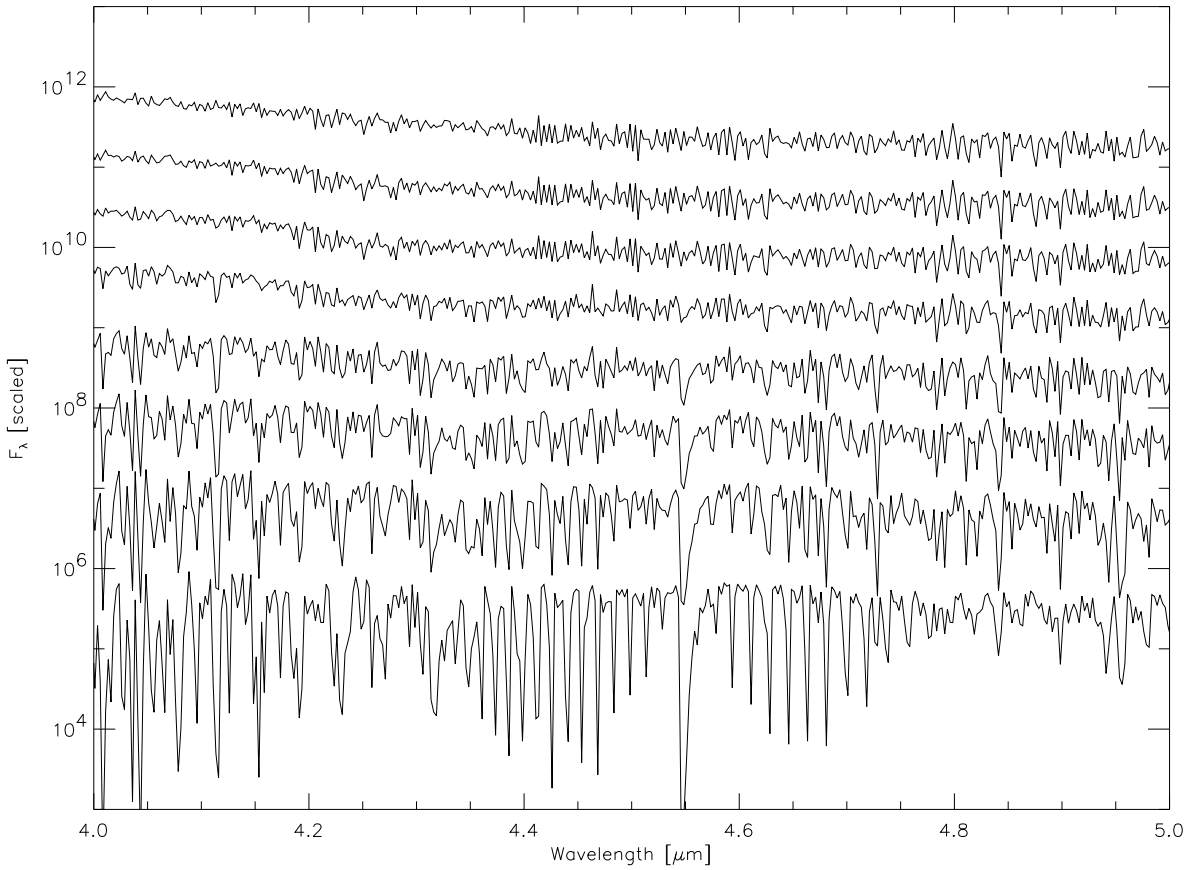

Fig. 12.— Same as Figure 10 where we zoom in on the CH_3D band system at 4.55 μm. From top to bottom: $T_{eff} = 2000, 1700, 1500, 1300, 1000, 800, 600,$ and 400K. The CH_3D band appears at 1000K at this gravity and for this dust treatment limit. Note that $T_{eff} = 2000$K dwarfs are dusty and that, though they don't appear here, CO bands at 4.67 μm easily **are** detectable in these hotter atmospheres.

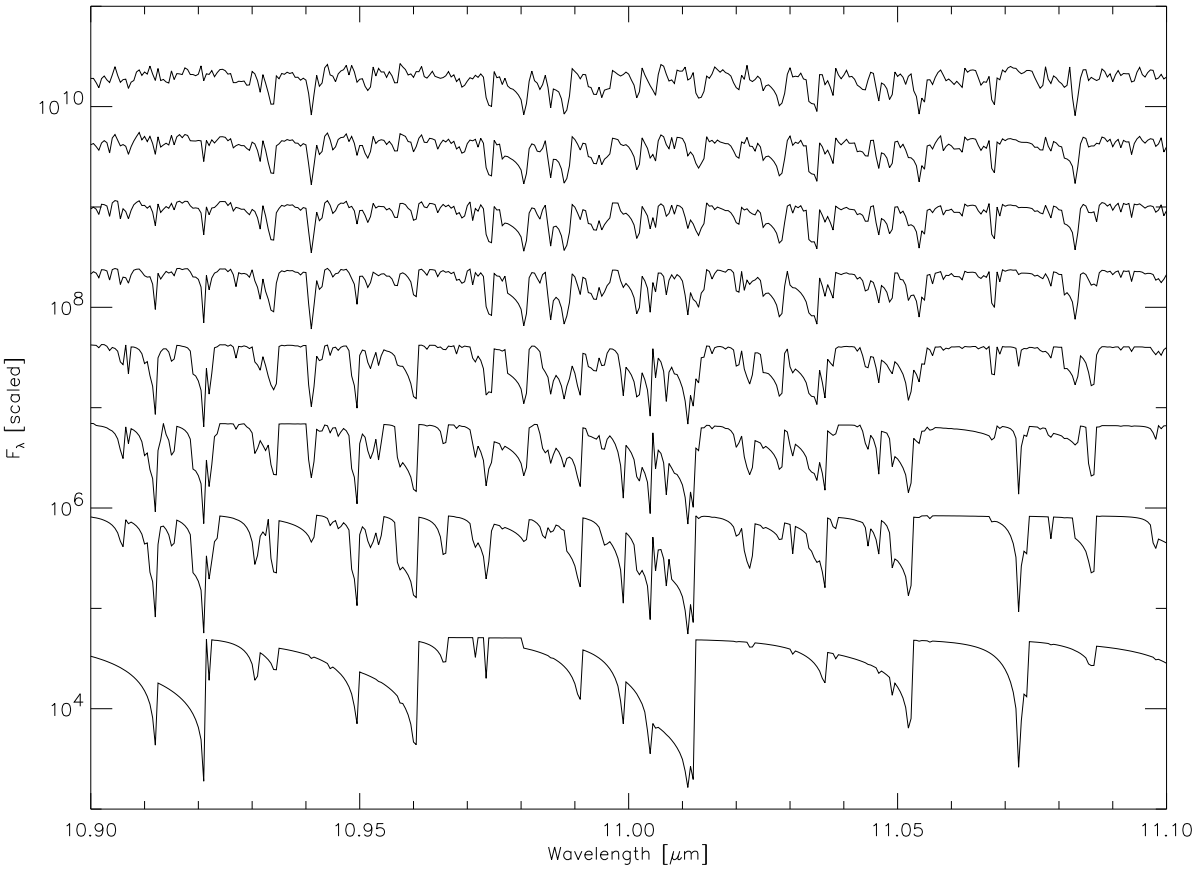

Fig. 13.— Same as Figure 10 where we zoom in on the NH_3 band system at 11.012 μm. The ammonia band system appears at 1000K, along with several other molecular lines essentially due to methane. The spectral resolution is 5Å.

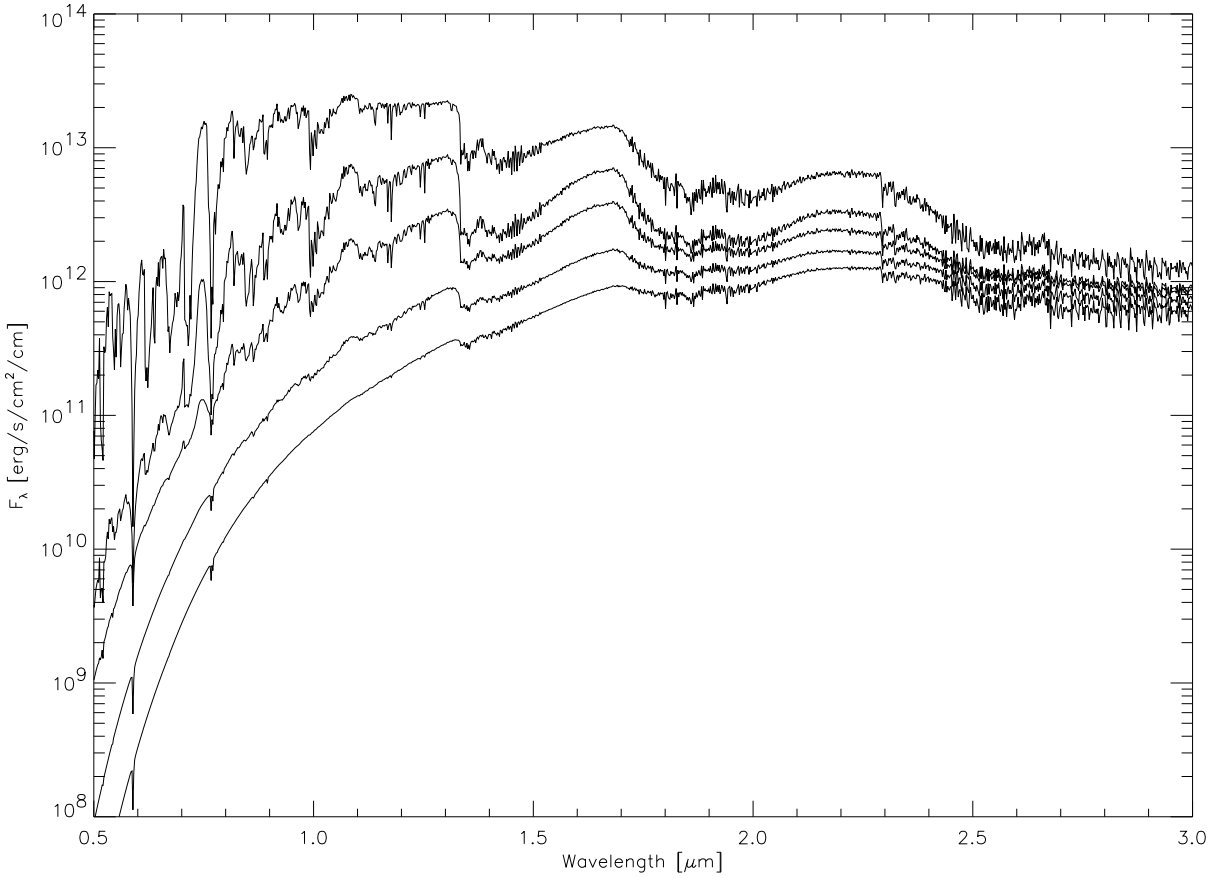

Fig. 14.— Same as Figure 8 in the full dusty (AMES-Dusty) limiting case. From top to bottom: $T_{\rm eff} = 2500, 2000, 1800, 1600$K, and 1500K. The gravity is fixed at $\log g = 5.0$. Here the strong heating effects of dust opacities prevent the formation of methane bands, and dissociate H_2O while producing a hotter water vapor opacity profile, much weaker and transparent to radiation. From 1700K, the grain opacity profiles rapidly dominate the UV to red spectral region, smoothing out the emergent flux into a continuum where only the core of the strongest atomic resonance lines (Na I D and K I doublets) are seen.

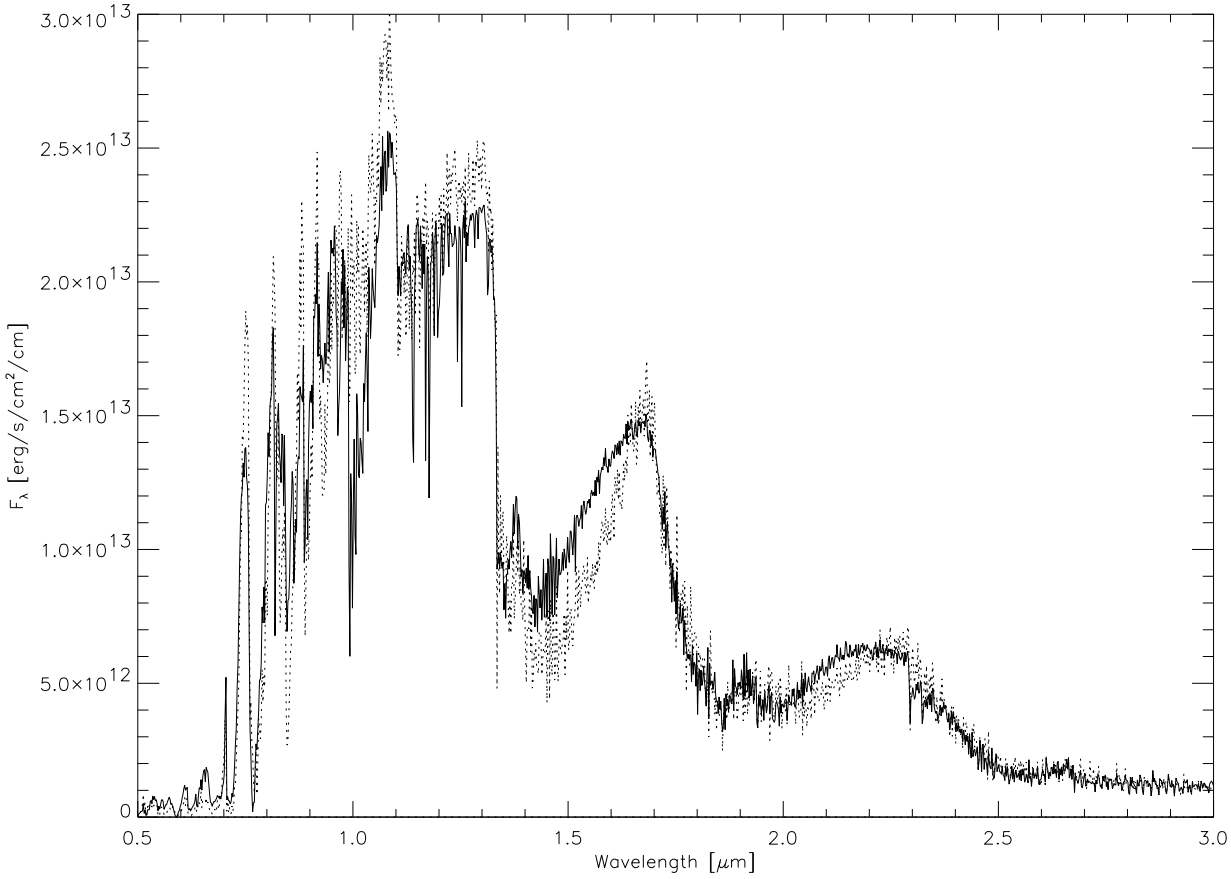

Fig. 15.— Two $T_{\rm eff}$ = 2500K AMES-Cond models of different surface gravity are compared: (1) $\log g = 5.5$ (full line), (2) $\log g = 2.5$ (dotted line). The spectral resolution has been reduced from 2Å to 10Å by boxcar smoothing in order to make comparison of the spectra easier.

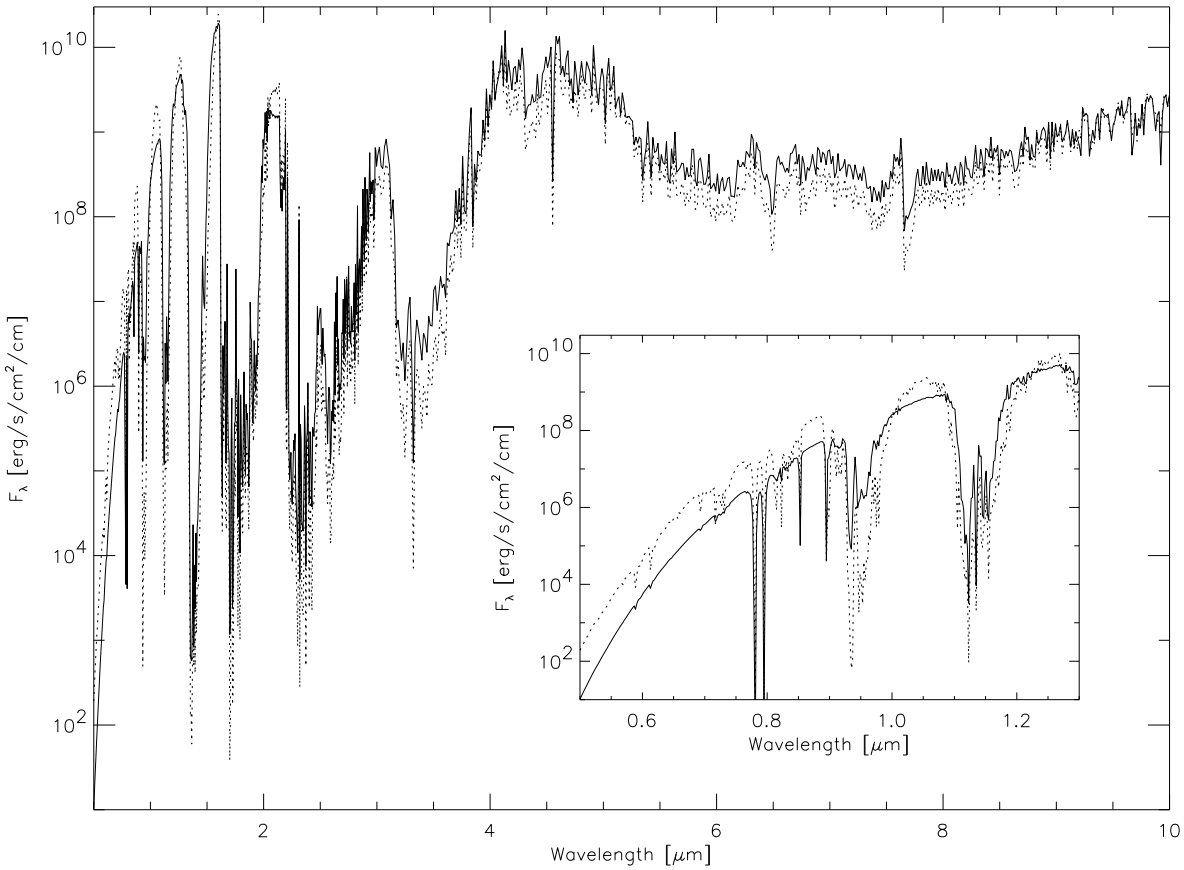

Fig. 16.— Same as Figure 15 for $T_{\rm eff}$ = 500K AMES-Cond models, and (1) $\log g = 4.0$ (full line), (2) $\log g = 2.5$ (dotted line). Here the spectral resolution has been reduced to 30Å by boxcar smoothing. In the inset we show a zoom of the optical to red spectral regime, were we distinguish water vapor bands at 0.93, 0.95 and 1.12 μm, Cs I resonance transitions at 0.86 and 0.89 μm, the K I resonance doublet at 0.77, 0.79 μm, and the cores of a few other lines such as the Na I D doublet bluewards of 0.75 μm. While molecular bands are moderately affected by the gravity change, the optical background opacity due to the wings of the Na I D and K I doublets is reduced by nearly a factor of 10 in the low gravity model. The latter model is more typical of low mass brown dwarfs and jovian planets.

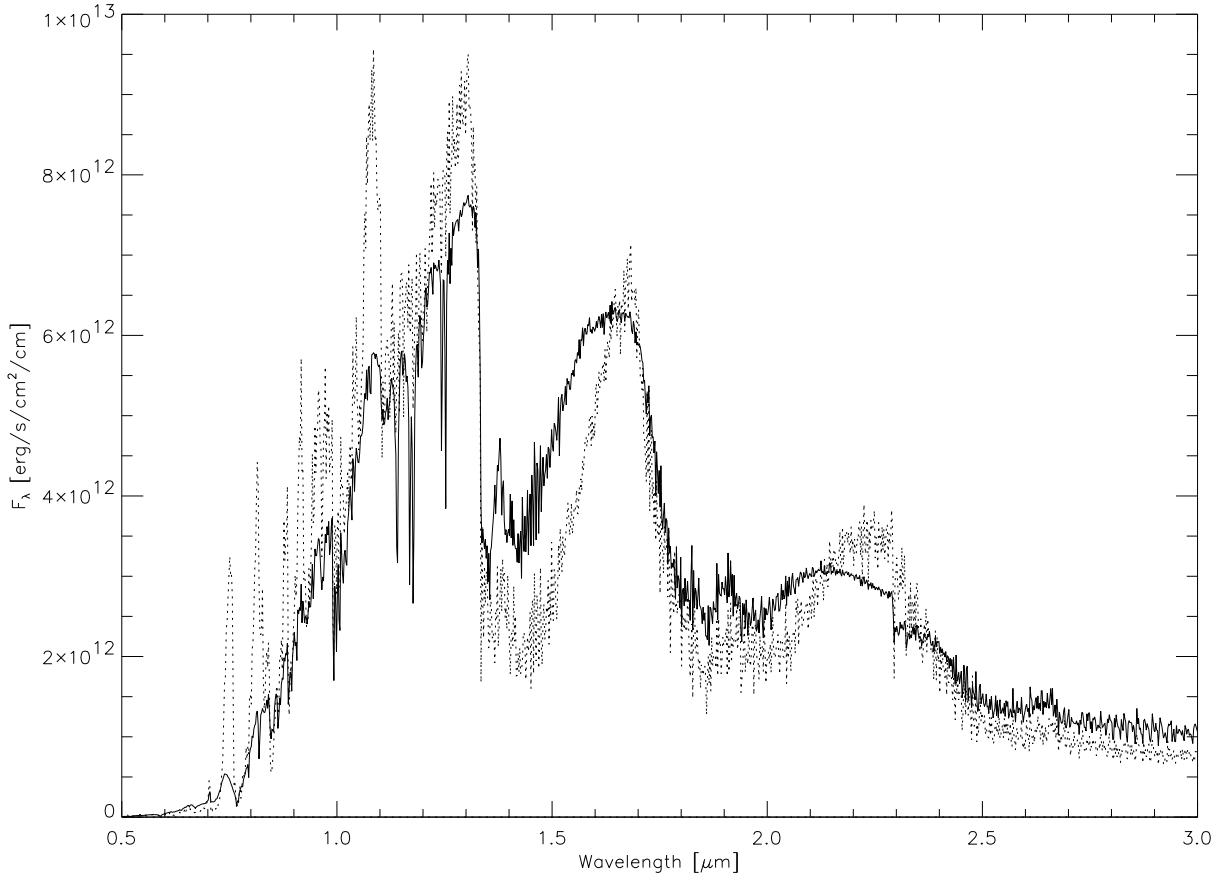

Fig. 17.— Two $T_{\rm eff}$ = 2000K AMES-Dusty models of different surface gravity are compared: (1) $\log g = 6.0$ (full line), (2) $\log g = 3.5$ (dotted line). The spectral resolution has been reduced to 10Å by boxcar smoothing.

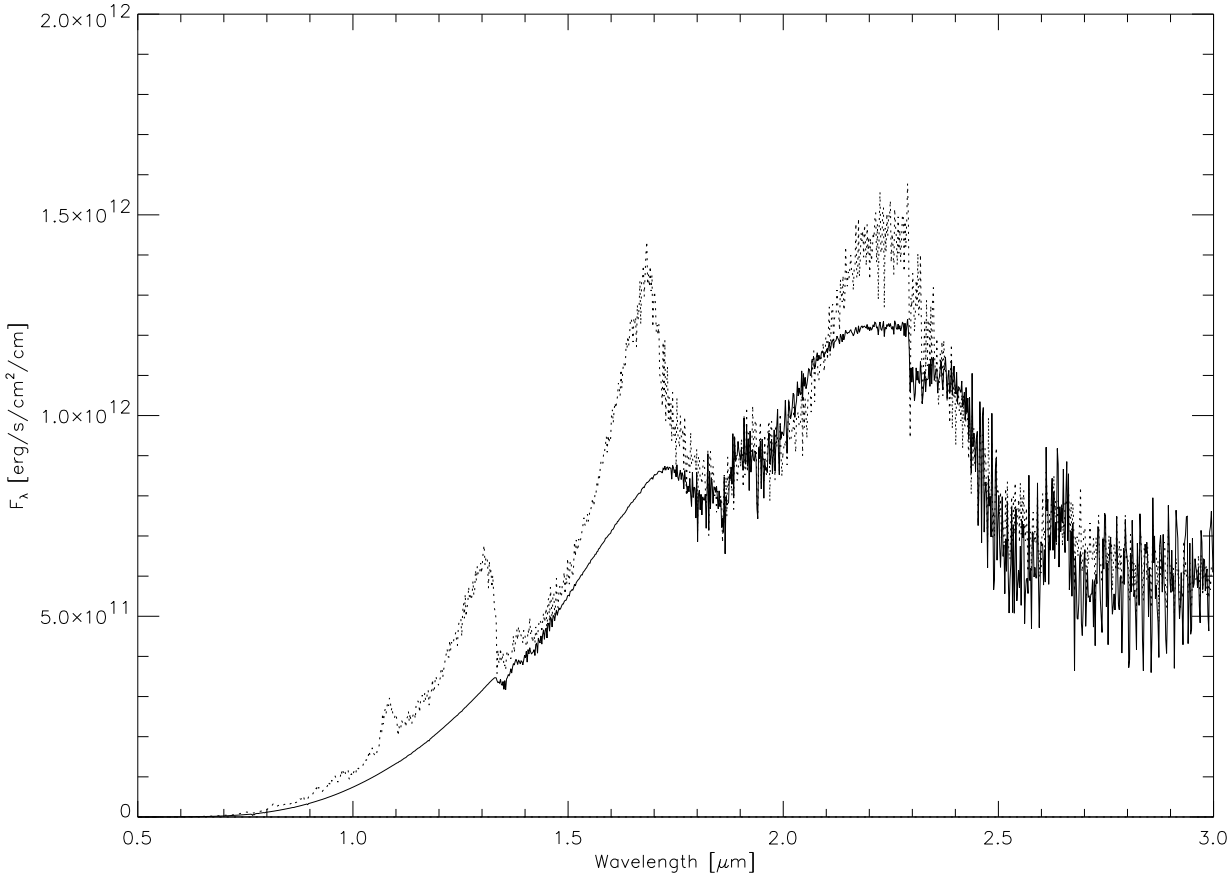

Fig. 18.— Same as Figure 17 for T_{eff} = 1500K AMES-Dusty models. While gravity effects are quasi nonexistent redwards of 2.5 μm, they are quite large in the optical to red spectral region, mainly as a result of enhanced efficiency of dust grain formation at the higher pressures and densities of high gravity atmospheres. A $\log g$-value of 5.5 is typical of most field brown dwarfs discovered since 1996.

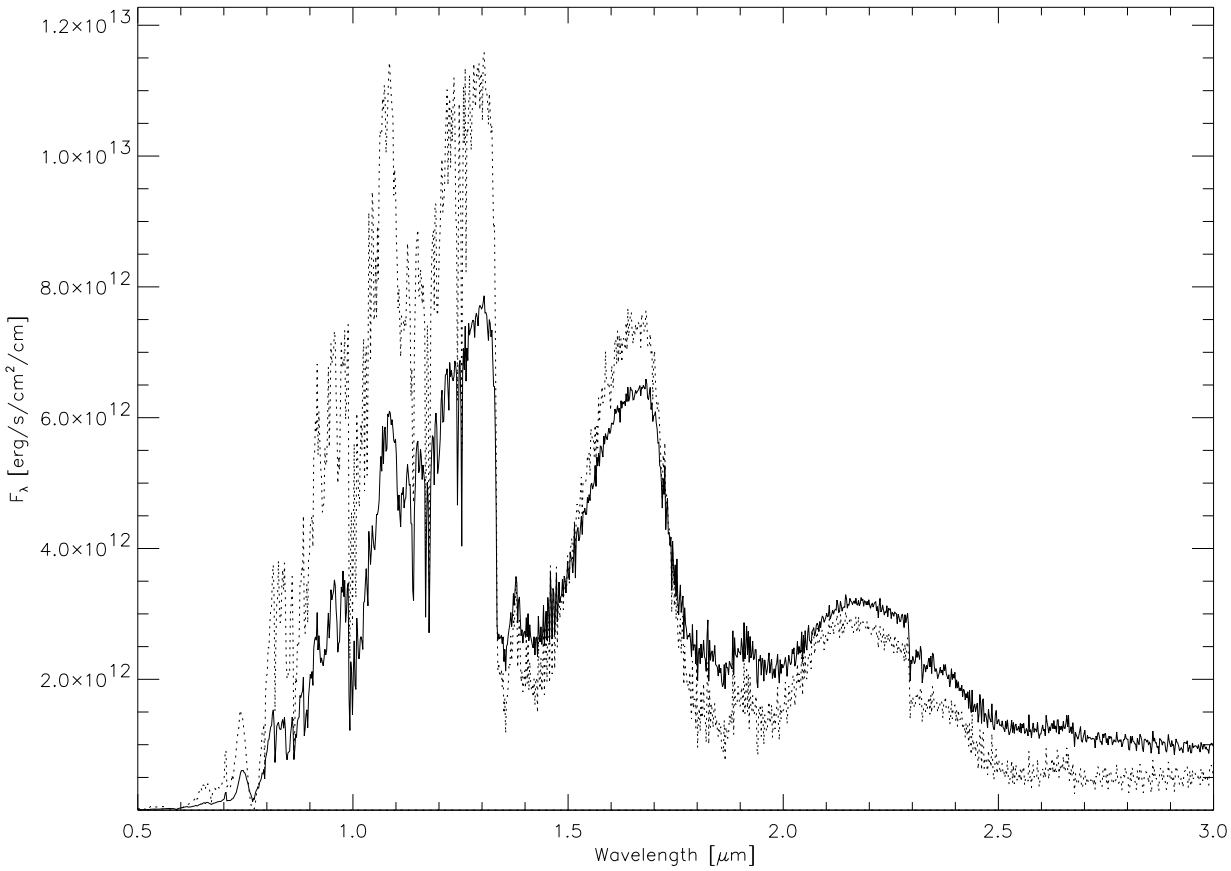

Fig. 19.— Two $T_{\rm eff}$ = 2000K models with $\log g = 5.5$ are compared to illustrate the difference between our two limiting cases: (1) AMES-Dusty with full dust opacity (full line), and (2) AMES-Cond with full gravitational settling (no dust opacity, dotted line).

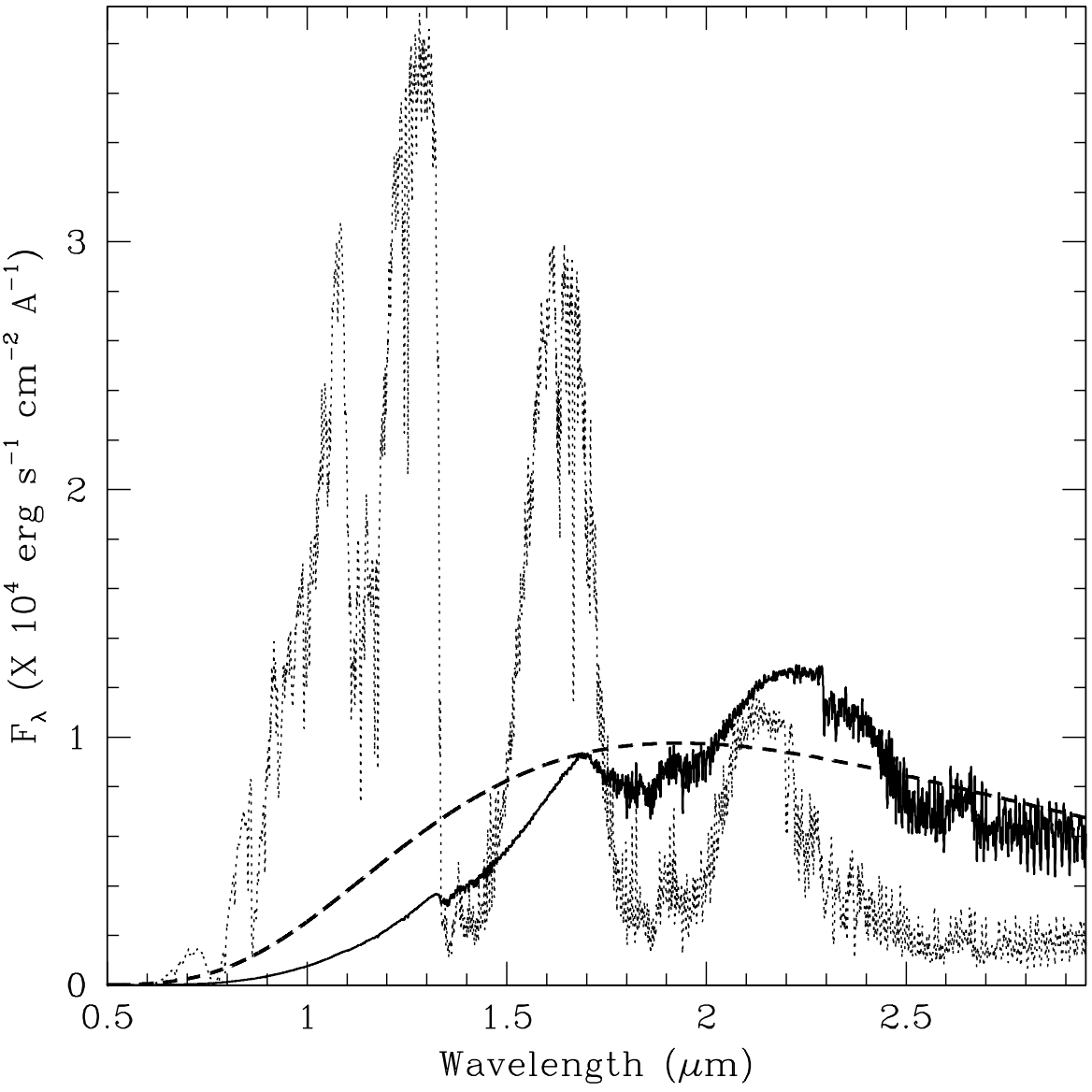

Fig. 20.— Same as Figure 19 for T_{eff} = 1500K models with $\log g$ = 5.0. A 1500K blackbody (dashed line) is overplotted for comparison.

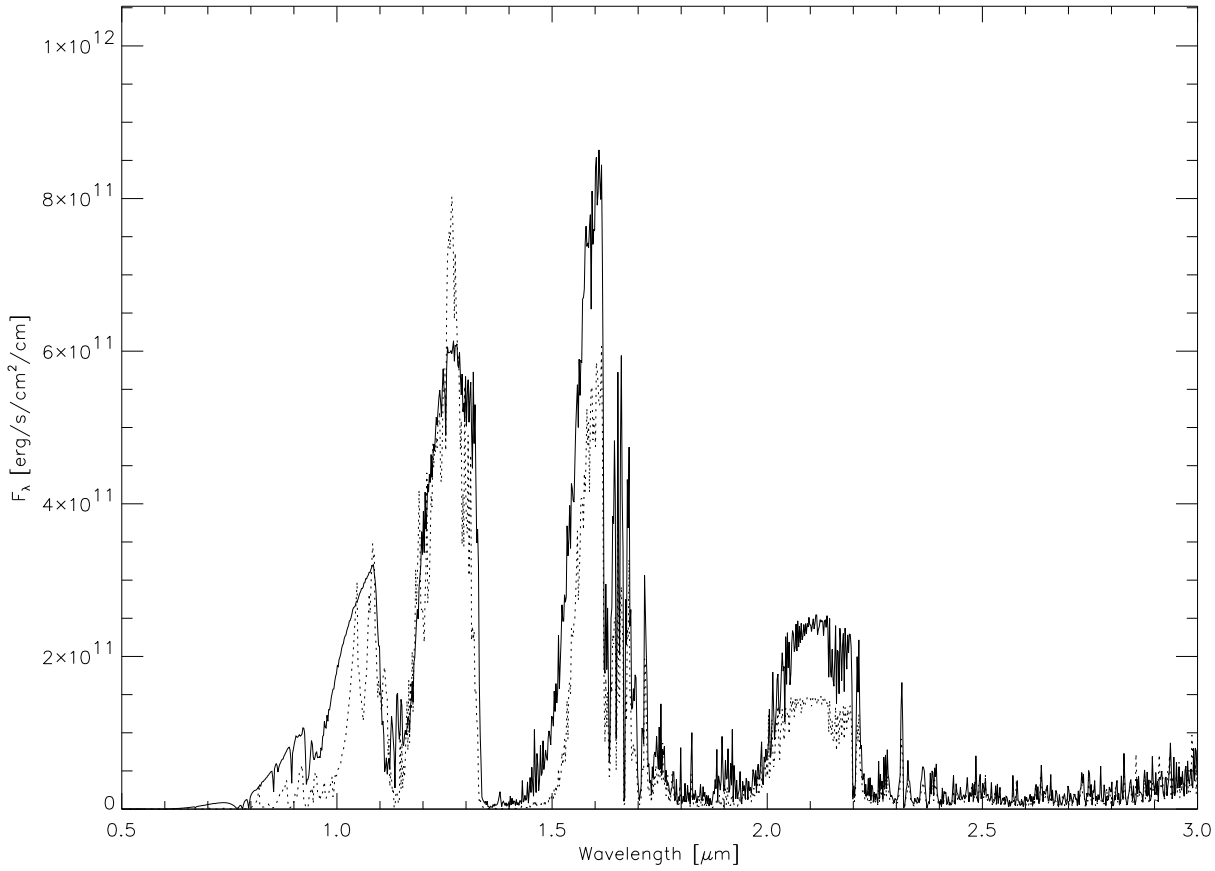

Fig. 21.— The AMES-Cond model for $T_{\rm eff}$ = 1000K and $\log g = 5.0$ (full line) is compared to the corresponding Allard et al. (1996) model (dotted line) used in their analysis of the Gl229B spectrum.

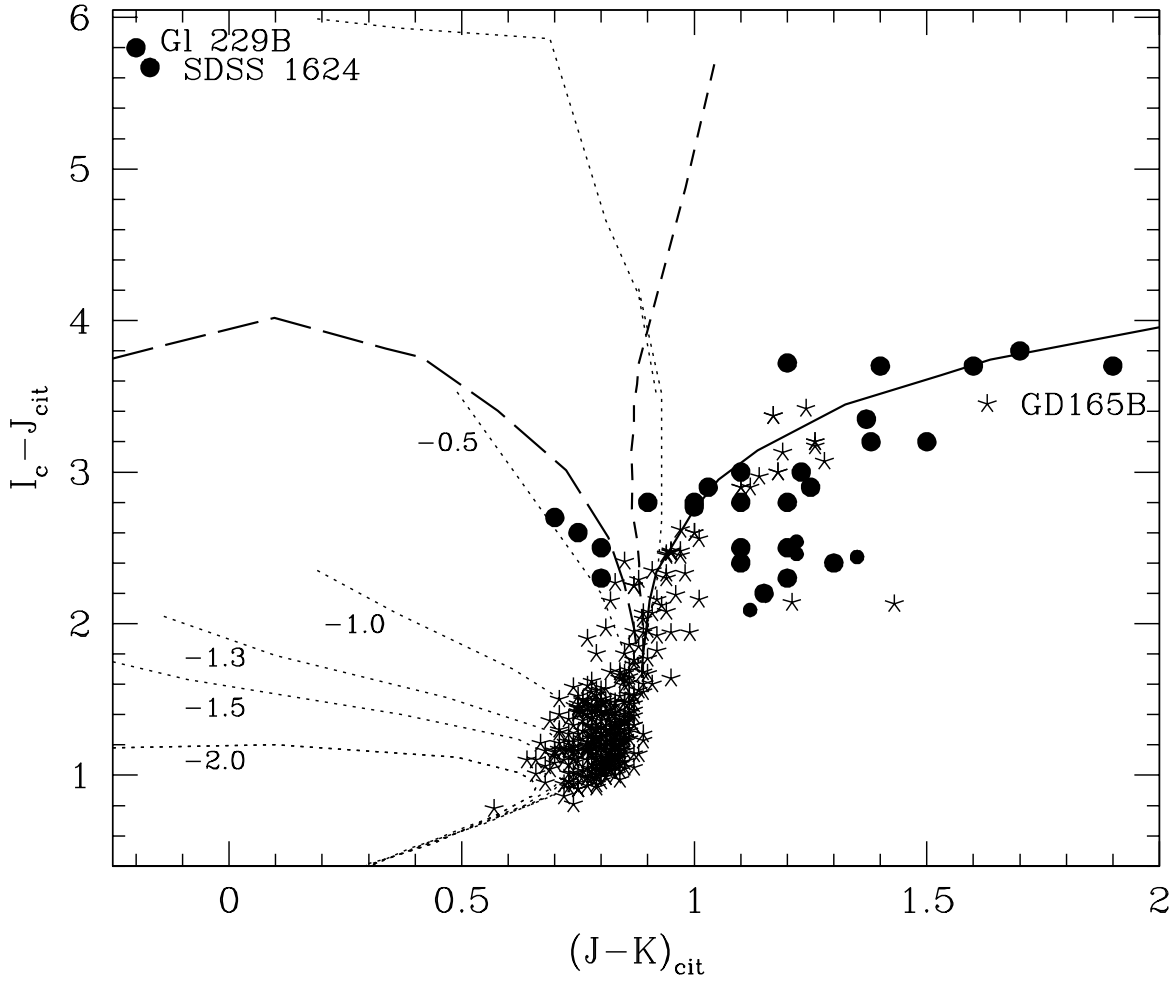

Fig. 22.— The 10 Gyr NextGen isochrones (dotted), and the $\log g = 5.0$ locii of the Cond (short dashed) and Dusty (full) models are compared to the photometric observations of field stars and brown dwarfs, and to Pleiades objects including the brown dwarfs PPl15, Teide1 and Calar3 (star and filled circle symbols). The field T dwarfs Gliese 229B and SDSS1624 are also shown. Unresolved binarity is reflected in this diagram by a red excess in $J - K$. Note that the Cond and Dusty models have been shifted in $J - K$ by +0.15 in order to eliminate water opacity source effects in this comparison. The Cond models are computed (i) with the line wings coverage value of 5000Å (long-dashed line), and (ii) with a maximum coverage of 15000Å (short-dashed line) to illustrate the impact of this parameter on the Cond models.